Report of the National Research Center for Disaster Prevention, No. 25, Marh 1981

550.34.01

On Migration Phenomena of Aftershocks Following Large Thrust Earthquakes in Subduction Zones

By

Masajiro Imoto

National Research Center for Disaster Prevention, Japan

Abstract

The spatio-temporal patterns of aftershock sequences following large thrust earthquakes in subduction zones are investigated in relation to tectonic environment. A prominent pattern of seaward spreading of quiescent areas during a period of about 10 days after the main shock is detected, in many cases with similar tectonics of typical subduction zones. The pattern is displayed in various ways such as in space-time plots, distribution of space and time intervals among the shocks, and variation of the frequency decaying rate with distance from the main shock. The sequences of elongated aftershock area suggest that the spreading starts at a line source along the landward side of the aftershock area.

To account for the process of migration, a stress analysis in the source region is made by a two-dimensional finite element method with a fault gouge in sequence, which may represent a realistic tectonic process at preseismic, coseismic, and postseismic stages. The result of stress analysis at a postseismic stage is compared with the observed data in four cases. The criterion used for the aftershock occurrence is that the frequency of aftershock in a certain area during a certain period is proportional to the increasing rate of the shear stress in the space and time intervals. Comparisons with the observed data result in success, and spatio-temporal distributions of the sequences can be explained quantitatively. A few related problems such as postseismic deformation, frequency decay law and others are also discussed on the basis of the results.

Contents

* *Seismic Activity Laboratory, Second Research Division*

1. Introduction

Aftershock sequences have long been a major field of research in seismology, ad a number of general properties of aftershock sequences have been found. Shallow tectonic earthquakes, regardless of their size, are almost always accompanied by aftershocks, whereas the same is not true for deep earthquakes. Utsu (1961) studied the time-frequency, magnitude-frequency (b value of Gutenberg-Richter's statistical formula), aftershock area-magnitude of the main shock relations and others. He reviewed previous studies on aftershocks and developed them (Utsu, 1969, 1970, 1971b, 1972). Recently, closer discussions have been made with more accurate deta. Yamakawa (1966, 1967a, b, 1968a, b) and Yamakawa *et al.* (1969) examined the clustering tendency of aftershocks in space and time and pointed out that randomness of activity is different for different periods. They also mentioned thet the period during which a spatial distribution is random is closely related to the period during which a frequency distribution is random.

On the other hand, several studies of spatial and temporal clustering of intermediate and deep focus earthquakes have been made. Isacks *et al.* (1967) investigated the spatial and temporal clustering of earthquakes in the Fiji-Tonga-Kermadec region. Oike (1971) researched clustering tendency in space and time of intermediate and deep earthquakes all over the world. He concluded that predominant time sequences of intermediate and deep multiplets are different from those of shallow earthquakes or swarms.

Mogi (1962c, 1963a, b) performed laboratory experiments on fracturing of rocks, and showed that patterns of earthquake sequences depend on heterogeneity of material, and the shape and depth of the source. He discussed the relation between the patterns of earthquake sequences and geotectonic structure in and near Japan. On the basis of fracture experiments under compressional stress, a possible mechanism for aftershock sequences was also discussed by Mogi (1962b) and Scholz (1968).

Besides research which discusses either general properties of aftershock sequences or spatial and temporal clustering, there exist innumerable papers which report individual activity of aftershocks. Among them, migration phenomena of aftershock activities have been sometimes reported with interest, but not clearly elucidated. Mogi (1968) reported rapid propagation of aftershock activities at the times of the Aleutian earthquake of March 9, 1957 and the Alaskan earthquake of March 28, 1964. Whitcomb *et al.* (1973) obtained a migration speed of 5-15 km/day for the San Fernando earthquake of February 9, 1971. Santo (1964), Yamakawa *et al.* (1972b), and Algermissen *et al.* (1972) also examined migrations of aftershock sequences. However, a property of migration obtained from one sequence is not always reproduced in another sequence.

Study of aftershocks plays important roles for the source study of their main

shock. It was pointed out that an aftershock area corresponds well to the area of crustal deformation (Kishinouye, 1936; Ishimoto, 1937) or the tsunami source area (Iida, 1956; Hatori, 1970). For these reasons, an aftershock area is usually considered to represent the source area of the main shock. Kellher *et al.* (1973) examined aftershock areas of some large earthquakes in the trenches of the Pacific Ocean and the Caribbean Sea, and tried to predict locations of large shallow earthquakes.

Though tectonics in various regions are interpreted through results of research into the source process, aftershocks are not sufficiently examined in relation to the source mechanism of the main shock or tectonic environment, except for some cases (Yamakawa, 1971, 1972, a; Whitcomb *et al.*, 1973).

In this paper, we will examine aftershock sequences with tectonical study as the background, and discuss the process of aftershock occurrence. We will discover new migration phenomena, that is, a seaward spreading of a quiescence area at a speed of 6-13 km/day, for many aftershock sequences after large thrust earthquakes in subduction zones. We will focus our attention on such sequences for the following reasons. Aftershock activity is more prominent for shallow earthquakes, and large earthquakes occur more frequently in subduction zones than in any other regions. Moreover, activity of thrust-type earthquakes is highest in a subduction zone, and the source process of the shock is better elucidated than in those of other types.

The present paper is composed of two parts : a display of data (Chapters 2 and 3) and a quantitative study based on a simple model (Chapters 4, 5 and 6). In Chapter 2, we will review tectonics in different regions and show some basic data. Spatio-temporal patterns of each aftershock sequence will be shown in Chapter 3. New patterns of seaward migration of a quiescent area will be discovered, and the migration will be shown in various ways. In Chapter 4, preliminary discussions will be made so as to build up a model which could account for spatio-temporal patterns. In Chapter 5, the source process in subduction zones will be simulated by a two-dimensional finite element method with fault gouges. The results from the simulations will be compared with the observed data in four cases of aftershock sequnces. In the discussion chapter, our model will be examined from various points of view, and we will probably be able to obtain more general aspects of aftershock occurrence.

2. Data

2.1 Data selection

The purpose of this paper is to study spatio-temporal patterns of aftershock sequences. Before displaying patterns and examining them, in this chapter we will review tectonics in the regions where aftershock sequences studied here are located.

The sequences studied here are aftershocks of large thrust-type earthquakes ($M \geqq 7$) that occurred in the trenches of the Pacific Ocean during the period from Oct. 1963 to Oct. 1974, followed by many aftershocks (more than 20, within 400 km and 30 days of the main shock). Earthquakes with magnitudes of less than 7 usually have a small number of aftershocks and a small source area (Utsu and Seki, 1955), so it is difficult to discuss aftershocks in this case.

Table 1 shows the source parmeters of the main shocks which triggered the present sequences. All the parameters of the main shocks and their aftershocks are taken from the *NOAA Earthquake Data File* and *Earthquake Data Report*, except for the magnitudes of the main shocks, from *Rikanenpyo* (1978). The fault plane solutions in earlier studies are referred to so as to select thrust-type earthquakes ; for

shocks without a solution, nodal planes are estimated here from the first P wave motion recorded by long-period seismographs of the WWSSN. The sequences which show newly discovered patterns are marked by an asterisk in the first column of the

Table 1 List of main shocks.

No.	Date (UT)	Location	Lat. (deg)	Lon. (deg)	Depth (km)	M	Extension along trench (km)	Reference
1*	1963 Oct. 13	Kuriles	44.8N	149.5E	60	8.1	-200~200	Kanamori, 1970a
2*	1964 Mar. 28	Alaska	61.0N	147.8W	33	8.4	-300~ 50	Kanamori, 1970b
3*	1964 July 24	Kuriles	47.2N	153.8E	33	7.0	-200~200	Stauder and Mualchin. 1976
4	1964 Nov. 17	New Britain	5.8S	150.7E	45	7.6	-150~150	Johnson and Molnar, 1972
5*	1965 Feb. 4	Aleutian	51.5N	178.6E	40	7.8	-300~100	Wu and Kanamori, 1973
6*	1965 Aug. 11	New Hebrides	15.5S	166.9E	14	7.0	-100~300	Johnson and Molnar, 1972
7	1966 Oct. 17	Peru	10.7S	78.8W	24	7.5	-200~200	Stauder, 1975
8*	1966 Dec. 28	Chile	25.5S	70.7W	32	7.8	-200~200	Stauder, 1973
9*	1967 Oct. 4	Solomon Is.	5.7S	153.9E	52	7.5	-200~200	Johnson and Molnar, 1972
10	1967 Dec. 25	Solomon Is.	5.3S	153.7E	64	7.0	-200~ 50	Johnson and Molnar, 1972
11*	1968 Jan. 29	Kuriles	43.7N	146.7E	40	7.0	-200~200	Stauder and Mualchin, 1976
12*	1968 May 16	Japan	40.8N	143.2E	7	7.9	-150~ 1	Kanamori, 1971a
13*	1968 May 20	Kermadec	30.7S	178.4W	46	7.9	-100~100	Johnson and Molnar, 1972
14	1968 June 12	Japan	39.5N	142.7E	44	7.2	- 50~ 1	WWSSN
15	1969 Jan. 30	Philippines	4.8N	127.4E	70	7.2	-150~-50	Fitch, 1972
16*	1969 Aug. 11	Kuriles	43.5N	147.4E	28	7.2	-200~200	Abe, 1973
17	1970 Jan. 10	Philippines	6.8N	126.7E	73	7.3	- 50~ 75	Fitch, 1972
18*	1970 Apr. 29	Middle America	14.5N	92.6W	33	7.0	-200~200	WWSSN
19*	1971 July 9	Chile	32.5S	71.2W	58	7.5	-200~200	WWSSN
20*	1971 July 14	Solomon Is.	5.5S	153.9E	47	7.7	- 80~200	Pascal, 1979
21*	1971 July 26	New Britain	4.9S	153.2E	48	7.5	-200~ 1	Ripper, 1975
22*	1971 Dec. 15	Kamchatka	56.0N	163.3E	33	7.3	-200~200	Stauder and Mualchin, 1976
23	1972 Jan. 23	New Hebrides	13.2S	166.4E	33	7.1	-100~100	WWSSN
24	1972 Feb. 29	Izu	33.3N	140.8E	56	7.2	-200~100	Ichikawa, 1973
25	1972 Nov. 2	New Hebrides	20.0S	168.8E	32	7.0	-100~100	Pascal *et a* ., 1978
26*	1972 Dec. 2	Philippines	6.5N	126.6E	33	7.3	-150~ 50	Seno and Kurita, 1978
27*	1972 Dec. 4	Izu	33.3N	140.7E	66	7.4	-200~ 20	Ichikawa, 1973
28*	1973 June 17	Kuriles	43.2N	145.8E	48	7.4	-200~ 1	Stauder and Mualchin, 1976
29	1973 Dec. 28	New Hebrides	14.5S	166.6E	26	7.5	-200~200	Chung and Kanamori, 1978
30	1974 Jan. 31	Solomon Is.	7.5S	155.9E	34	7.0	-200~200	WWSSN
31	1974 Oct. 3	Peru	12.3S	77.8W	13	7.5	-200~200	WWSSN

table.

In regions near the trenches, the structure of seismic wave velocities is quite complicated and the location of earthquakes is systematically different when based on data from a different seismograph network (Utsu, 1967, 1971a). Sykes (1966) mentioned that the computed location was about 25 km north of the actual position on the basis of the Aleutian explosion. Mitronovas *et al.* (1969) reported that the locations of Tongan earthquakes based on teleseismic data alone fall 20 to 30 km west of the locations obtained with data from both local and teleseismic stations. In the present paper, we will use the parameters determined from one network and discuss relative, horizontal locations among aftershocks with an accuracy of about 20 km so the accuracy seems to be satisfactory. Necessary care is given to this point and to the detection capability in which most of the aftershocks with magnitudes greater than 4.5 can be located (Yamakawa *et al.*, 1969; Imoto and Kishimoto, 1977).

2.2 Peru-Chile

The left hand side of Fig. 1 shows the epicenters of four major earthquakes in the Peru-Chile region and their fault plane solutions projected onto the lower hemisphere of the focal sphere, and the histograms on the right hand side indicate the number of aftershocks during the period of the first 10 days and next 20 days (shaded) against the horizontal extent normal to the trench axis. Asterisks beside sequence numbers indicate sequences which show newly discovered patterns. Several sequences with other types of large main shocks are omitted here, because they are of a normal fault (Abe, 1972) or a thrust fault in the continental plate (Stauder, 1975), and not of thrust faults in accordance with subductions. As can be seen in the figure, two of them (Nos. 7 and 31) occurred in Peru and the others in northern (No. 8) and southern Chile (No. 19).

Seismicity and focal mechanisms of the western margin of South America have been discussed by Isacks (1970), Isacks and Molnar (1971), Stauder (1973) and Isacks and Barazangi (1977). There are appreciable differences among the Wadati-Benioff

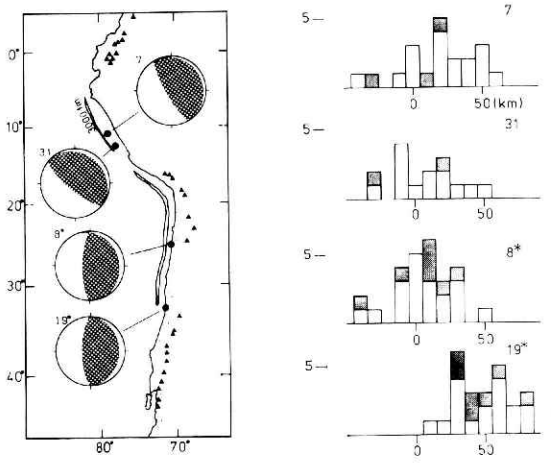

Fig. 1 The epicenters and mechanisms for main shocks in the Peru-Chile region and distributions of their aftershocks. The fault planes are projected onto the lower hemisphere of the focal sphere, and shaded areas are quadrants of compressional first motions. Solid triangles indicate active volcanoes. Depth contours are in fathoms. Histograms indicate the number of aftershocks during the period of the first 10 days and the next 20 days (shaded) against the horizontal extent normal to the trench axis. The positive direction of the abscissa is set seaward. Each main shock is located at 0 km. Asterisks beside sequence numbers indicate sequences showing migration phenomena. These contours and volcanoes in Figures 1-10 are after Molnar and Sykes (1969), Plafker (1969), Chase (1971), Kelleher and McCann (1976), Sclater *et al.* (1976) and Pascal (1976).

profiles beneath Peru, and northern, central and southern Chile as shown by Isacks and Barazangi (1977). They mentioned that the nearly flat Wadati-Benioff zones in Peru and central Chile have a remarkable correlation with the absence of Quaternary volcanoes, and suggested that generation of andesitic volcanism requires a wedge of asthenosphere between the subducted and upper plates. On the contrary, the Wadati-Benioff zones under northern and southern Chile where two sequences (Nos. 8 and 19) occurred, show straight descending slabs with somewhat steeper dips than those in Peru and central Chile.

The epicenters of the main shocks are located rather landward of their aftershock areas, as has already been pointed out by Kelleher *et al.* (1973) and Imoto and Kishimoto (1977a). Aftershocks Nos. 7 and 31 occurred over a wide area in low density as compared with Nos. 8 and 19, and No. 31 in particular seems to have a small number of aftershocks for its magnitude in spite of the best capability of detection with the most recent seismograph network among the four in this region.

2.3 Middle America

Molnar and Sykes (1969) reported that the oceanic plate is underthrusting towards the northeast beneath Mexico and Middle America. In this subduction zone, only one shock suitable for this study occurred on April 29, 1970. Fig. 2 shows the epicenter, the focal mechanism and width of its aftershock area. The focal mechanisms referred to are those given by Molnar and Sykes (1969). Aftershocks occurred in an area of 100 km or less in width and about 150 km in length. This size is moderate for the aftershock area of large shocks in this region (Kelleher *et al.*, 1973). The Wadati-Benioff zone under this shock reaches 200 km and even deeper. This region shows typical characteristics of island arcs with several geophysical features such as down-dip extensional mechanisms for intermediate-depth earthquakes (Isacks and Molnar, 1971), volcanic line and others.

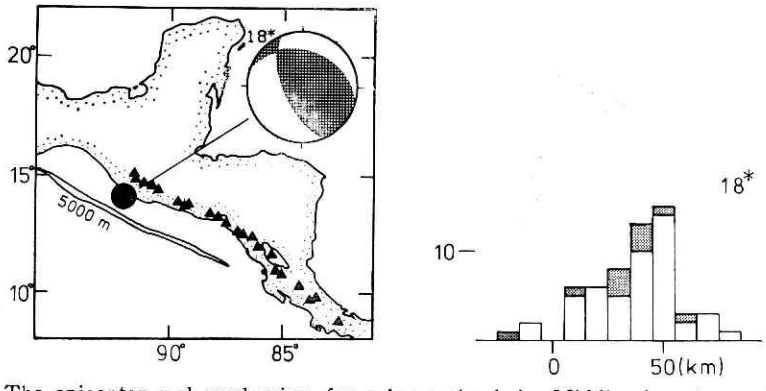

Fig. 2 The epicenter and mechanism for a large shock in Middle America and distribution of its aftershock.

2.4 Alaska-Aleutians

Alaska : The Alaskan earthquake of May 28, 1964 is one of the largest earthquakes in history. Many researchers have studied this shock from different kinds of data and by various methods (Press, 1965 ; Savage and Hastie, 1966 ; Stauder and Bollinger, 1966 ; Wyss and Brune, 1967 ; Mikumo, 1968 ; Plafker, 1969 ; Harding and Algermissen, 1969 ; Kanamori, 1970b ; Ben-Menahem *et al.*, 1972 ; Miyashita and Matsu'ura, 1978). From the results of these studies, it was found that the source area was 600～800 km long and its strike was 25°～55° NE. Miyashita and Matsu'ura (1978) determined

the parameters of three faults striking southwest and dipping northwest, and one fault located on the northeastern part of the aftershock area striking northwest and dipping northeast. In accordance with these solutions, regional variations of the focal mechanism of aftershocks had already been reported by Stauder and Bollinger (1966).

Mogi (1968) pointed out a rapid southeastward migration of large aftershocks ($M \geqq 6$) at a speed of about 60 km/h within 10 hours after the main shock. Algermissen *et al.* (1972) also examined spatial (along the trench axis) and temporal patterns of the sequence but any clearer patterns were not detected.

In this paper, taking regional variations of the focal mechanisms into consideration, we select aftershocks that occurred in the area shown in Fig. 3 (within two broken lines). In later sections, spatio-temporal patterns of this sequence will be examined in detail by various methods.

Aleutians: The Rat Island earthquake of Feb. 4, 1965 is another recent large earthquake. Wu and Kanamori (1973) have studied the source process of this event. On the basis of the radiation patterns and the amplitudes of long-period surface waves, the dip and strike of the fault were found to be 18° and N71°W respectively. Stauder (1968) determined a part of the focal mechanism solution for the main shock and solutions for many large aftershocks. These solutions for the aftershocks located in the inner zone of the trench indicate that the landward block overthrusts the oceanic side.

Melosh (1976) reported a seaward migration of this sequence within about 3,000 days after the main shock. He obtained the starting line of migration which obliquely encountered the trench, by a least squares fit to the epicenters of the aftershocks, but only those located on the seaward side of this straight starting line were examined. The lower side of Fig. 4 shows the number of aftershocks against the horizontal extent of their distribution to the direction normal

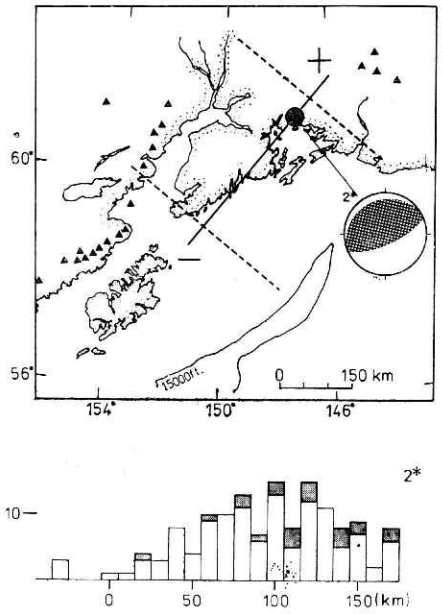

Fig. 3 The epicenter and mechanism for the Alaskan earthquake and distribution of its aftershocks. Two broken lines indicate the limits of studied aftershocks. The distances of limits from the main shock along the trench are entered in the fifth column of Table 1. The positive direction of the column is set counterclockwise at 90° from the seaward direction, and is indicated by a + mark in the figure. The depth contour is in feet.

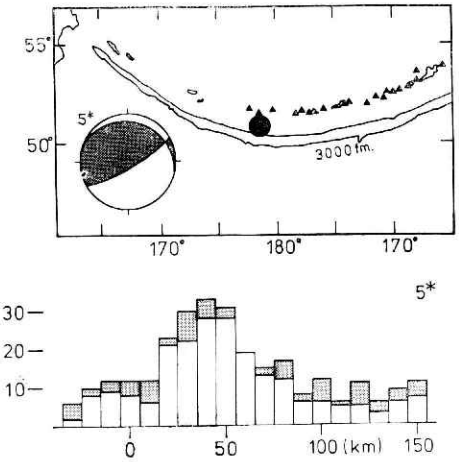

Fig. 4 The epicenter and mechanism for the Ret Island earthquake and distribution of its aftershocks.

to the trench axis. The straight line in Melosh's paper seems to be located around the 50 km mark in Fig. 4. It is to be mentioned here that there are pronounced differences between Melosh's data and those in this paper in a few respects : one is the location of aftershocks and another is their time interval, 3,000 days in Melosh's paper and ten days or so in this paper. In later chapters, differences in migration features and their interpretation will be discussed.

2.5 Kuriles-Kamchatka

The Kurile-Kamchatka region is seismically one of the most active regions. Recently, many large earthquakes have occurred along the southern part of the Kurile Trench (see Fig. 5). In addition to the high seismicity of large earthquakes, their aftershock activity is also characterized by their large scale (Santo, 1970b). There have been many investigations into these earthquakes (Kanamori, 1970a ; Abe, 1968 ; Shimazaki, 1974 ; Imoto, 1976), and their aftershocks (Santo, 1964 ; Mogi, 1968 ; Maki, 1968 ; Yamakawa *et al.*, 1969). Imoto and Kishimoto (1977a) mentioned that most of the main shocks with thrust-type faults along trenches are located landward in their aftershock area, and that this tendency is prominent in the Kuriles. Imoto and Kishimoto (1977b) also examined aftershock sequences in this region and suggested seaward migrations of aftershock activities.

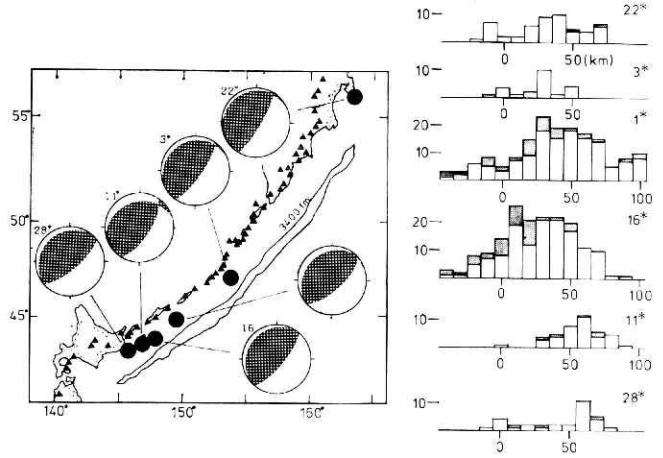

Fig. 5 The epicenters and mechnisms for main shocks in the Kurile-Kamchatka region and distributions of their aftershocks.

Among the sequences studied here, No. 1 was followed by the largest aftershock with a magnitude greater than 7, about a week after the main shock. The largest aftershock of No. 1 was located at 100 km east of the main shock, and the location of aftershocks following this largest event was hardly distinguishable from that of the prior shock. Fukao (1979) studied this largest event and defined it as a tsunami earthquake. On the contrary, the secondary aftershocks after the largest aftershock of No. 28 are easily distinguished from prior aftershocks by their locations. From another point of view, the secondary aftershock activity was extremely high at a stage of decreasing frequency of the first group of aftershocks. Utsu (1961) pointed out that the activity of secondary aftershocks is much lower than that of aftershocks of a single earthpuake with the same order of magnitude. It may be suggested that this secondary pactivity is weakly related to the main shock No. 28. In this paper, such secondary activity as in the case of No. 28 will be omitted, and activity in the case of No. 1 is included.

2.6 Japan

In the Japan Trench and its adjacent region, four aftershock sequences are

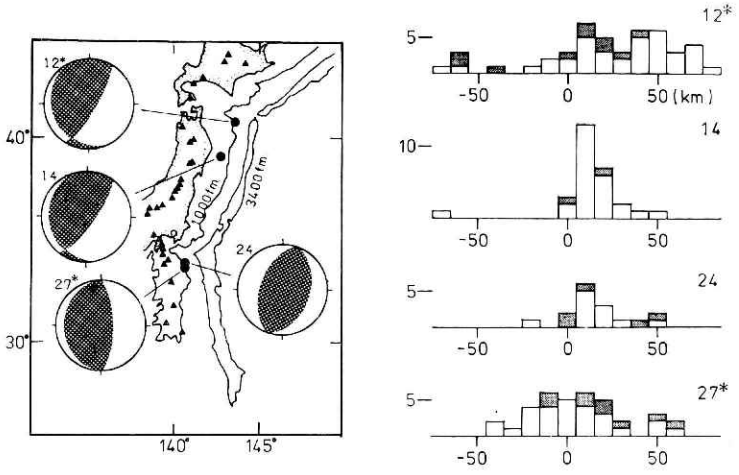

Fig. 6 The epicenters and mechanisms for main shocks near Japan and distributions of their aftershocks.

studied as seen in Fig. 6. Nos. 14 and 27 took place closely to Nos. 12 and 24, respectively. Kanamori (1971a) reported that shock No. 12 occurred at the junction of the Kurile and Japan trenches. The largest aftershock occurred at a trough which branches off towards the northwest from the Junction, and has a different mechanism from that of the main shock, with an almost opposite slip direction. Other small aftershocks that occurred in the neighborhood of the largest aftershock indicate a mechanism similar to that of the largest aftershock. For this reason, aftershocks located to the north of main shock No. 12 are excluded here.

An earthquake, No. 14, which seems to be the second largest aftershock of No. 12, occurred about a month after No. 12. The aftershock area of No. 14 overlaps the southern portion of that of No. 12. However, there is a contrast in the frequency of aftershocks just before and right after this shock, that is, the aftershock activity of No. 14 is too high to be the secondary aftershock of No. 12. Yamakawa and Kishio (1972) mentioned that this second largest aftershock is one of the aftershocks not directly triggered by No. 12. Subsequently, only aftershocks of No. 14, which were located closely to its epicenter, were also studied as an independent sequence. As can be seen in Fig. 6, the aftershock area of No. 14 is less wide than that of No. 12.

Nos. 24 and 27 occurred close together and have similar fault plane solutions (Ichikawa, 1973). Aftershocks of No. 24 are located northeast of the main shock and those of No. 27 are mostly southeast of No. 27. The aftershock area of No. 27 is wider than that of No. 24.

2·7 Philippines

Fitch (1972) showed that the Philippine sea plate is subducting west-

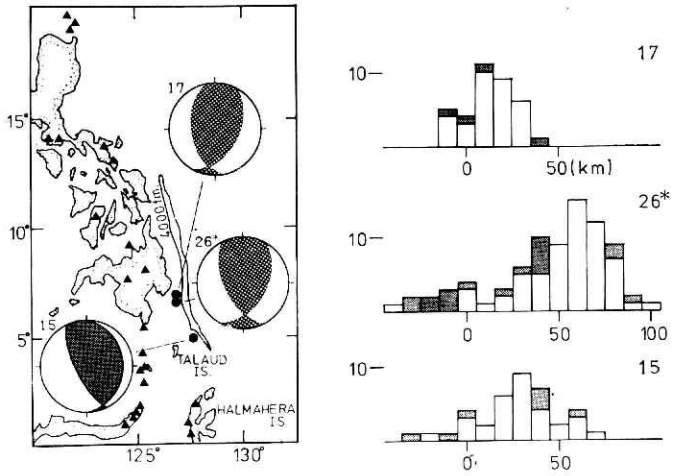

Fig. 7 The epicenters and mechanisms for main shocks in the Philippines and distributions of their aftershocks.

ward from the Philippine trench. A seismically active area along this trench branches off into two parts in the southern part of Mindanao Island, near Talaud Island, and extends to the west and northeast of Halmahera Island. A Wadati-Benioff zone under Mindanao Island reaches a dapth of 200～300 km (Seno and Kurita, 1978). Intermediate-depth earthquakes show down-dip extensional focal mechanisms. However, in the southeastern part of the branch the tension axis for intermediate-depth earthquakes tends to be more nearly vertical (Isacks and Molnar, 1971). Earthquakes Nos. 17 and 26 studied here, occurred close together at the northern part of the branch, and No. 15 at the southeastern part. The aftershock area of No. 17 is less wide than that of No. 26.

2.8 New Britain-Solomons

Johnson and Molnar (1972) mentioned that the Australian plate is subducting towards east-northeast under the Solomon Islands and north-northwest under New Britain Island. Intermediate-depth earthquakes show down-dip extensional focal mechanisms (Isacks and Molner, 1971). The Wadati-Benioff zones show continuous profile to a depth of about 200 km. Seismicity at intermediate-depths here is lower than that beneath other island arcs (Pascal, 1979). Fig. 8 shows the horizontal extents of aftershock areas. At first sight, it seems that the main shock is not always located landward of its aftershock area, for example, in the case of No. 30. However, considering the fact that the New Georgia Islands where No. 30 occurred are characterized by rather abnormal features of gravity, bathymetry and volcanoes (Johnson and Molnar, 1972), No. 30 may well be regarded an exception.

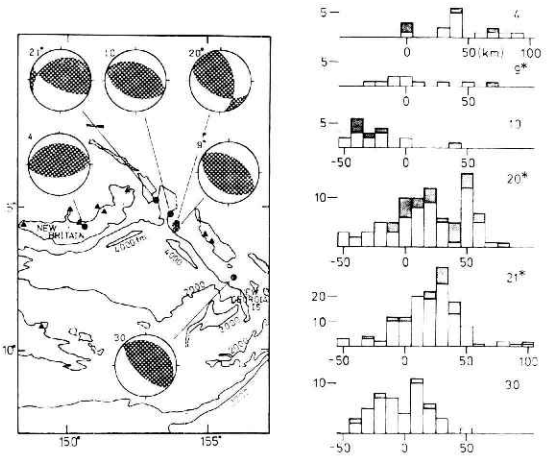

Fig. 8 The epicenters and mechanisms for main shocks in the New Britain-Solomon Islands region and distributions of their aftershocks.

2.9 New Hebrides

The Australian plate is subducting towards ENE beneath the New Hebrides arc (Johnson and Molnar, 1972). Seismicity of shallow and intermediate-depth earthquakes indicates a planar Wadati-Benioff zone with a steeply dipping angle (Isack and Molnar, 1971). In the central part of this island arc, the D'Entrecasteaux fracture zone appears to intersect the New Hebrides arc almost at a right angle and seems to extend to the east of the trench. The aftershock sequences of Nos. 6 and 29, each of which contains a few larger shocks with magnitudes greater than 7 in a swarm, are bounded at the latitude of 15.2°S, by an eastward extension of the fracture zone. Chung and Kanamori (1978) inferred that this is a surface manifestation of a structural boundary in the subducted fracture zone at depth. At the extension of this zone, the activity of intermediate-depth earthquakes is higher and shows a less steep angle for the Wadati-Benioff zone, and their depths are shallower than in adjacent regions (Santo, 1970a ; Chung and Kanamori, 1978).

As can be seen from the right hand side of Fig. 9, the main shocks (or triggered events) are commonly located near the centers of the aftershock areas along the

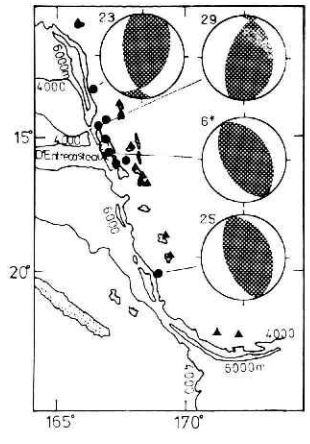

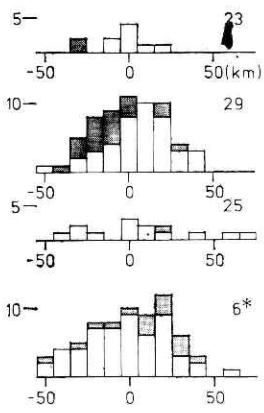

Fig. 9 The epicenters and mechanisms for main shocks in the New Hedrides and distributions of their aftershocks. Depth contours are in meters.

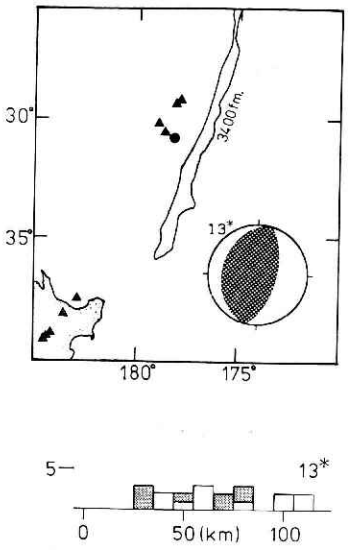

Fig. 10 The epicenter and mechanism for a large shock in Kermadec and distribution of its aftershocks.

direction normal to the trench. However, it is questionable to conclude that landward locations of the main shocks relative to their aftershock areas cannot be seen in this region, since Nos. 6 and 29 occurred in the exceptional region above mentioned, and Nos. 23 and 25 are less active than Nos. 6 and 29.

2.10 Kermadec

In the Tonga-Kermdec region, the Pacific plate is subducting westward (Isacks *et al.*, 1969). Isacks and Mȯlnar (1971) showed down-dip extensional mechanisms of intermediate-depth earthquakes at a depth of about 230 km.

Fig. 10 shows the epicenter of the shock studied here (above) and the width of its aftershock area (below). The main shock is located further landward with respect to the extreme land-side of its aftershock area. This tendency may also be seen in two other smaller sequences which occurred about 2 and 4 months after this sequence, in adjacent areas.

3. Spatio-temporal patterns

3.1 Space-time plots

In the preceding sections, we examined possible relations between the location of the main shocks and their aftershock area in several subduction zones, and it was found that the main shock is generally located on the landward side of its aftershock area rather than on the seaward side. From this fact, it is speculated that the source area of the main shock and its aftershock area may be in nonuniform fields of some parameters closely related to shear fracture such as the shear stress, shear strength, etc.. This nonuniformity may be reflected in spatio-temporal patterns of aftershock activities. For some sequences, migrations of aftershock activities have

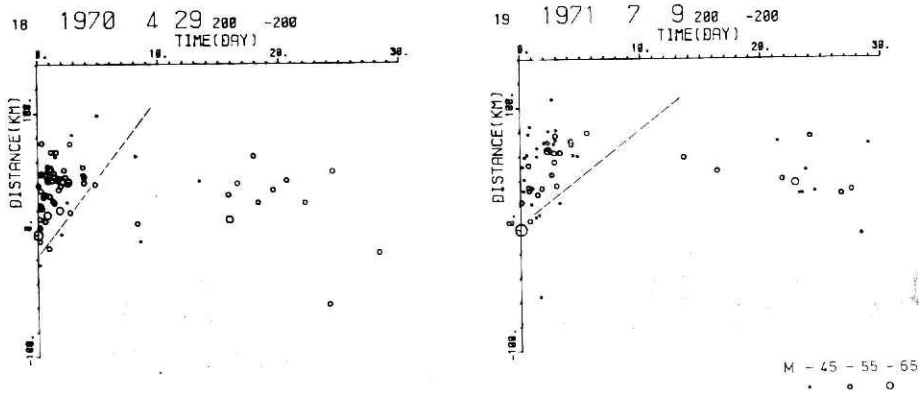

Fig. 11 Examples of space-time plots. The ordinate is the distance from the main shock normal to the trench and directs seaward. The abscissa is time after the main shock. The straight lines in the plots indicate linear approximations for the theoretically determined fronts of **SSQA** in section 5.5. The space-time plots for all sequences are shown in Appendix 1.

also been reported (Melosh, 1976 ; Imoto and Kishimoto, 1977a). In this chapter, spatio-temporal patterns of aftershock activities given in Table 1 will be examined using various methods.

First, a qualitative view of spatio-temporal patterns will be made using space-time plots. Fig. 11 shows two examples of the plots. In these plots, epicenters of aftershocks are projected on a line normal to the trench axis. The ordinate indicates the projected distance from the main shock which is taken positive seaward, and the absissa indicates the time elapsed after the main shock, respectively. The largest circles at the origin time indicate the main shock. All these plots for the sequences given in Table 1 are shown in the Appendix 1.

It can be seen from Fig. 11 that a quiescent area of aftershock activity starts at some point near the main shock epicenter and spreads seaward at a speed of about 10 km/day. Hereafter, we shall call this type of migration *"Seaward Spreading of Quiescent Area"* (**SSQA**). Dashed straight lines in Fig. 11 and the Appendix 1, which are determined by a method described in a later section, 5.5, indicate fronts of the quiescent areas.

SSQA may be seen in many plots in the Appendix 1, for instance, No. 18 in Middle America, No. 2 in Alaska, No. 5 in the Aleutians, No. 11 in Kurile and so on. In these plots **SSQA** appears generally more clearly on the landward side than on the seaward side. This evidence suggests that the source of **SSQA** is rather near to the land side of an aftershock area. However, several sequences do not show **SSQA** so clearly, and a few of them do not show it at all. The sequences showing **SSQA**, which are marked by an asterisk in the first column of Table 1, are located in regions with typical characteristics of island arcs such as deep trenches, volcanic lines, gently dipping Wadati-Benioff zones which reach 200 km and even deeper, and down-dip extensional mechanisms for intermediate-depth earthquakes. On the contrary, several remarks on the latter sequences which do not show **SSQA** are given as follows.

(1) Nos. 7 and 31 occurred in Peru, where volcanoes are absent.

(2) Nos. 14 and 24 have focal mechanisms similar to those of Nos. 12 and 27,

respectively, but the aftershock areas of the former sequences are smaller than those of the latter.

(3) No. 17 occurred at the branch of the Philippine trench where the tension axis for intermediate-depth earthquakes is near vertical.

(4) No. 30 is located on a somewhat abnormal subduction zone near the New Georgia Island.

(5) Nos. 6 and 29 also occurred in the vicinity of an anomalous part of the New Hebrides arc. It seems that **SSQA** can be found after the last larger shocks ($M \geq 7$) in the sequence of No. 6.

In later sections where we will build up our model to elucidate **SSQA**, these conditions under which **SSQA** is not rec ognized will be also taken into consideration.

At the end of this section, an important characteristic of **SSQA** will be examined on the basis of a set of space-time plots. The aftershock area of the Rat Island earthquake (No. 5) is 500～600 km wide along the Aleutian trench. The space-time plot for this sequence over almost the whole region is shown in the Appendix 1. The aftershock area is divided into several portions according to the distance from the main shock along the trench axis, and the space-time plots of these subareas are examined. Fig. 12 shows the space-time plots in three

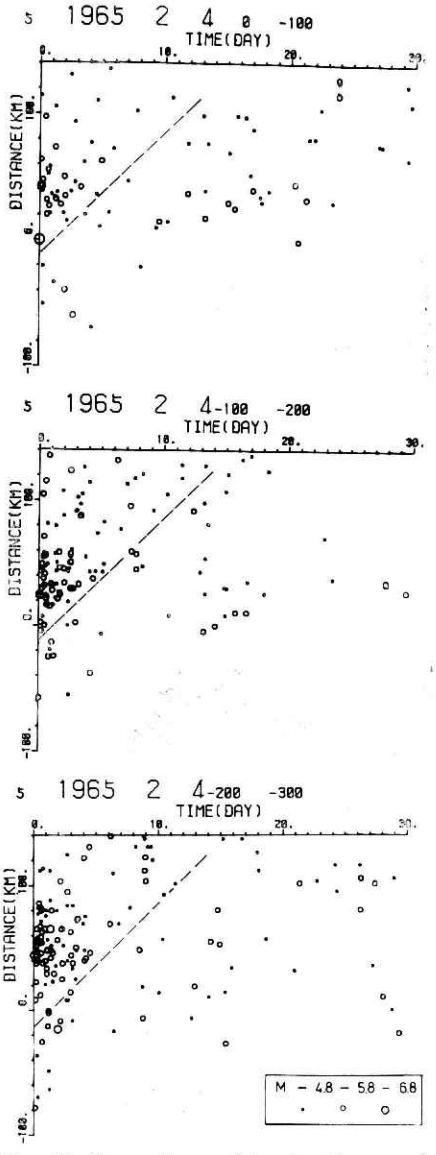

Fig. 12 Space-time plots in three sub-areas divided according to distance along the trench for the Ret Island sequence (No. 5). The ranges of the sub-areas are indicated by two numbers (in km) at the top of each plot.

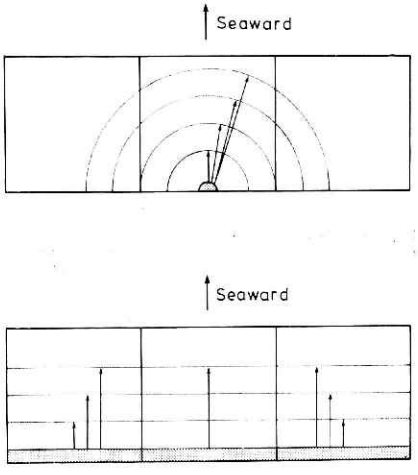

Fig. 13 Schematic figures of source models for **SSQA**. Shaded areas indicate a point source (upper) and a line source (lower). Half circles and straight lines are fronts of **SSQA** at certain instants.

distance ranges, 0～−100, −100～−200, and −200～−300 km. Each of these figures clearly shows **SSQA**, and it is found that these cases of **SSQA** commonly start at some point near the origin and spread at a similar speed, about 10 km/day. If **SSQA** starts from a point source and spreads with a circular front, the arrival time of **SSQA** in an area 100 km away from the source must be about 10 days later than that of an area including the source. On the contrary, if **SSQA** starts from a line source and spreads unilaterally, **SSQA** in each area, including a portion of the line source must show almost identical features. Judging from Fig. 12 and those of other sequences, the quiescent area is more likely to start from a line rather than a point source. In order to explain a possible mechanism of **SSQA**, this evidence would play a quite important role, that is, it suggests that **SSQA** may be treated as a two-dimensional problem with respect to the two directions vertically and horizontally normal to the trench axis.

3.2 Space-time intervals between aftershocks

Up to this point, aftershock areas and their space-time plots have been examined only with respect to the direction normal to the trench axis. However, the directions of rupture propagation in the main shocks have been reported in many cases to be nearly parallel to trenches (Kanamori, 1970a, b; Wu and Kanamori, 1973), and rapid migrations of aftershocks reported by Mogi (1968) also indicate directions parallel to trenches. From another point of view, there exist so many cases in which an aftershock area is wide in the direction parallel to the trench rather than in the normal direction. Taking these points into consideration, it is necessary to inspect aftershock activities not only in the direction normal to the trench but also in other directions. In this section, three sequences (Nos. 2, 5, and 21) will be examined, especially on the above mentioned point, by methods not so subjective as in the previous section, but more objective, which have been used by Imoto and Kishimoto (1977b).

If earthquakes in a sequence show propagational activity exactly in one direction, the apparent velocity between every two earthquakes,

$$\Delta v_{ij}=\Delta x_{ij}/\Delta t_{ij}$$

where

Δx_{ij} : distance interval between event i and j

Δt_{ij} : time interval between event i and j

will be the propagation velocity of the events. On the contrary, in a sequence that shows no propagative features, the apparent velocity may scatter over a wide range. In this case, the frequency distribution of Δv_{ij} is expected to be symmetric with respect to the origin in any range of space interval or time interval (Imoto and Kishimoto, 1977b).

Each diagram of Fig. 14 shows frequency distributions of Δx_{ij} for every pair of aftershocks in a time interval $2 \leqq \Delta t_{ij} < 3$ (days). Vectors Δx_{ij} in a polar coordinate system are classified into four groups for their azimuths and three groups for their distances by a 30 km step. A possibility of migrations, if it exists, will be indicated by asymmetricity with respect to the origin. Comparison between two abjacent groups in their azimuths does not appear to give any clear information for migration phenomena. As seen clearly in the cases of Nos. 5 and 21 and to some degree in the case of No. 2, Δx_{ij} distributes more frequently in the seaward direction than in the opposite direction, while the groups in two different orientations parallel to the trench show no appreciable asymmetricity. If we assume a unilateral migration, seaward migration appears more obvious than in any of the other three directions. But the azimuths here have a large resolution of $\pm 45°$. However, if we take smaller

divisions for the azimuths to depress the estimated errors, the result would become less reliable because of more scanty data involved in each group.

Hereafter, a modified method is used on the basis of another parameter and the seaward migration will be further investigated. A combination of two parameters, Δt_{ij} and scalar Δx_{ij} (defined as a projection of vector Δx_{ij} in a certain direction) is examined here. Figs. 15, 16 and 17 show frequency distributions of Δt_{ij} for every pair of all aftershocks in the distance range, $30 \leqq \Delta x_{ij} < 60$ or $-60 < \Delta x_{ij} \leqq -30$ (km) for the cases of Nos. 2 and 5, and $15 \leqq \Delta x_{ij} < 45$ or $-45 < \Delta x_{ij} \leqq -15$ (km) for the case No. 21. Six subsets in each sequence correspond to six different azimuths counted at every 30° clockwise from the dircetion parallel to the trench. The distributions of Δx_{ij} in opposite orientations are overlapped in each subset for convenience of comparison. The histograms with small + marks on the top indicate the distributions in the case where Δx_{ij} directs outward, and those without + marks indicate the opposite

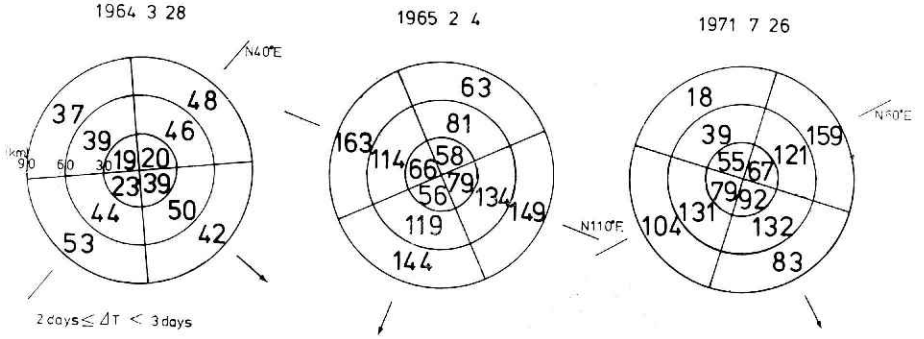

Fig. 14 Distributions of space-time intervals for three sequences (Nos. 2, 5, and 21) of numerous aftershocks. Each diagrom shows frequency distributions of distance intervals for every pair of aftershocks in a time interval of greater or equal to 2 and less than 3 days. Distance intervals in the polar coordinate system are classified into four groups for their azimuths, and three groups for their distances in 30 km steps. Each aftershock used for counting is within 200 km of its main shock normal to the trench and the range shown in Table 1 along the trench, and has a magnitude 4.5 and above. The strike of the trench and seaward direction (arrow) are also indicated for each sequence.

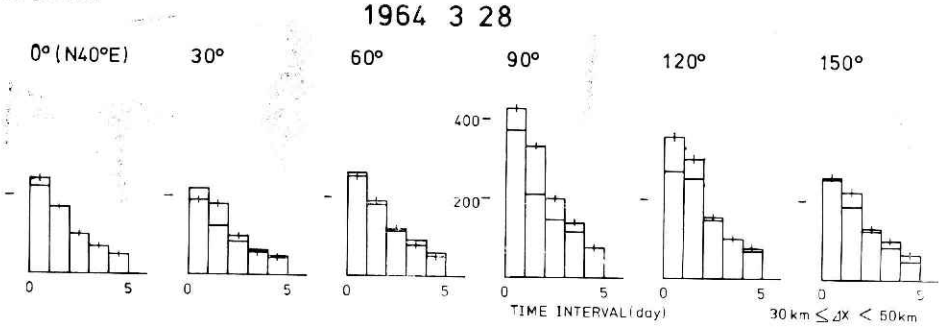

Fig. 15 Distributions of space-time intervals for the Alaskan sequence (No. 2). In figures 15—17, the distance intervals of each two aftershocks are projected in six directions at every 30°. The number above each histogram indicates this direction of projection counted clockwise from the strike of the trench. A pair whose distance interval is equal to or greater than 30 km and less than 60 km is classified according to its time interval. The histograms counting the pairs orienting outwards to the arc are marked by a + mark on their top, and those without + marks are oriented in the opposite direction. The data set is the same as that of Fig. 14.

direction, i. e. inward. Migration phenomena may be more easily noticed from the difference between the histograms with and without ÷marks. In each sequence, there is a most prominent difference in the fourth subset, corresponding to the case of a 90° direction, and very small difference in the case of a 0° direction, parallel to the trench. In the case of 90°, the distribution of distance intervals is more frequent outwards than inwards. On the basis of these results, it may be concluded that the direction of migration is more likely to be normal to the trench axis, with an error of within ±15°.

Imoto and Kishimoto (1977b) have investigated several sequences in the southern Kuriles, especially sequences Nos. 16 and 28 by the same methods, and have reported the same result as obtained here.

3.3 Variation of frequency decay with distance

Among many histograms given in the 2nd chapter, there are many cases in which aftershocks occurred less frequently near their main shock than at some distance from it. Under this spatial distribution of activity, if aftershock activities at various distances satisfy a formula of frequency decay, it is possible that the activity ceases earlier in a location nearer to the main shock. If this is true, **SSQA** may be only an apparent phenomenon and a spatial distribution itself may be more meaningful. One of the purposes in this section is to estimate whether **SSQA** is significant or not. Another purpose here is to examine **SSQA** quantitatively and to provide available data for study on mechanisms of **SSQA**. Two sequences, No. 2 in Alaska, No. 5 in the Aleutians, and a superposition of sequences in the southern Kuriles, Nos. 1, 11, 16 and 28, are inspected by the following method.

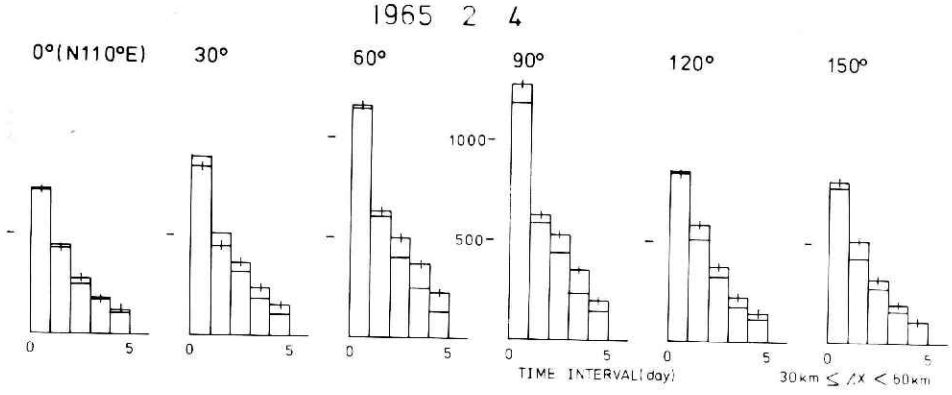

Fig. 16 Same as Fig. 15 but for the Rat Island sequence in the Aleutian region (No. 5).

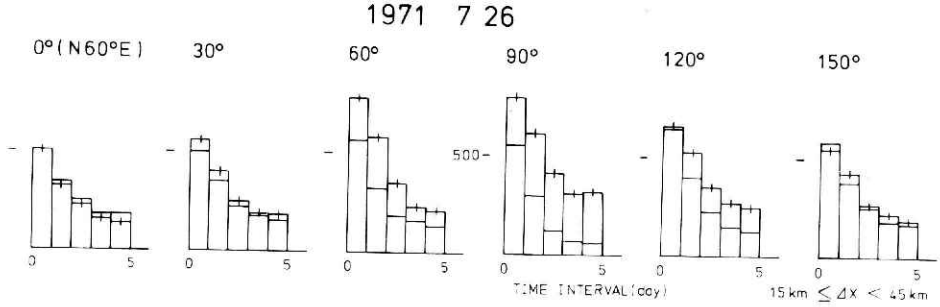

Fig. 17 Same as Fig. 15 but for the sequence in New Britain (No. 21).

The density of aftershock occurrence, $P(x, t)$, is defined here as the total number of shocks, each of which is located at (x_i, t_i), and satisfies the following relation.

$$\left(\frac{x_i-x}{L}\right) + \left(\frac{t_i-t}{T}\right)^2 \leqq R^2$$

where x indicates the distance from the main shock normal to the trench axis. In order to consider the variations of frequ ency decay with distance, $P(x, t)$ at x is normalized by $P(x, 0)$ which is the density of aftershocks right after the main shock. Hereafter, we will use this normalized value for the density with the same notation.

Figs. 18, 19 and 20 show time variations of $P(x, t)$ at various points. In the case of No. 2, L, T, and R are taken as 15km, 1 day, and 1, and in the other cases, 10 km, 1 day, and 1, respectively. For counting $P(x, t)$ and obtaining its smooth variation with time, the large number of aftershocks are needed for different parameters of smaller L, T and R. Each of Nos. 2 and 5 has sufficient number of shocks if L, T and R are taken with the above values. Although the number of shochs, Nos. 1, 11, 16 and 28, is not sufficient, they have nearly the same width of aftershock area in the direction normal to the Kurile trench, and their

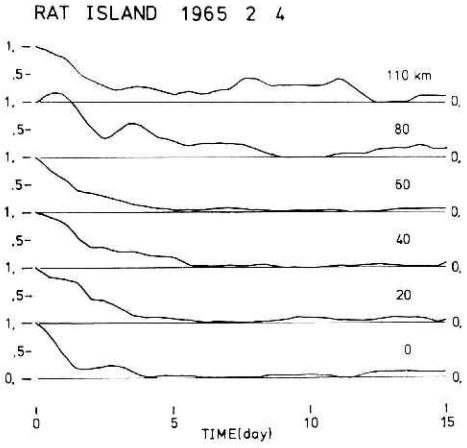

Fig. 19 Same as Fig. 18 but for Rat Island sequencein the Aleutian region (No. 5). The constants of the inequality are $L=10$ km, $T=1$ day and $R=1$.

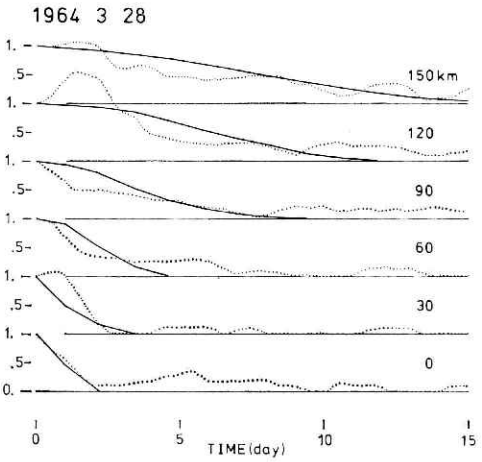

Fig. 18 Frequency decay curves at various distances for the Alaskan sequence (No. 2). The total number of shocks at (x_i, t_i) which satisfies the inequality.

$$\left(\frac{x_i-x}{L}\right)^2 + \left(\frac{t_i-t}{T}\right)^2 \leqq R^2$$

defines the frequency at (x, t). The constants of the inequality are $L=15$ km, $T=1$ day and $R=1$. Each curves at every 30 km is normalized by its initial value at $t=0$.

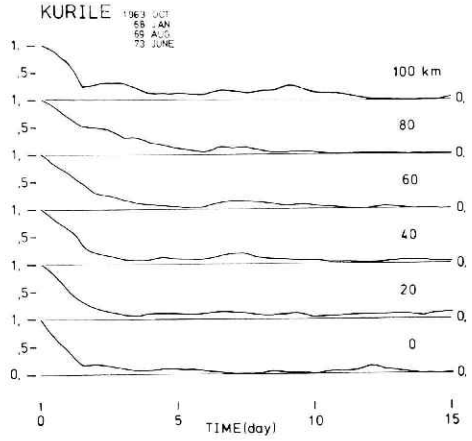

Fig. 20 Same as Fig. 18 but for the Kurile data containing four sequences (Nos. 1, 11, 16 and 28). The constants of the inequality are $L=10$ km, $T=1$ day and $R=1$.

focal mechanisms are similar to one another. Since the mechanism of aftershock occurrence is also likely to be similar, we may superpose these four sequences. As can be seen in all three cases given in these figures, the rate of frequency decay is different for different locations. The rate is highest near the main shock (the land side of aftershock area), and the frequency decay becomes slower in proportion to the distance measured seaward from the main shock.

These figures remind us of an elaborate work which was done by Utsu (1962). He showed that if the fracture rate with a form of exponential decay varies from region to region and satisfies a certain distribution, the modified Omori's formula can be derived.

It may be concluded that by an application of the smoothing technique proposed here for the spatio-temporal patterns of aftershock sequences, very important characteristics of **SSQA** have been detected. **SSQA** may not only be an apparent phenomenon, but can be interpreted to have physical meanings in that the frequency decay of aftershocks varies from point to point in one sequence and that the decaying rate is slower in the outer part of an aftershock area.

4. Fault gouge model

4.1 Model selection for spatio-temporal patterns

In the preceding chapters, we studied the characteristics of aftershock sequences following large thrust earthquakes in subduction zones, and the main results are described as below.

(1) A main shock is located on the landward side of its aftershock area rather than on its seaward side.

(2) **SSQA** can be recognized in many cases.

In the following two chapters, we will attempt to provide possible explanations for the above two phenomena. Several investigations related to the above two problems will be reviewed in order to elucidate the process of aftershock occurrence, and numerical modeling will be outlined to account for these phenomena.

An aftershock area has generally been considered to cover the fracture zone of the main shock, and the epicenter of the main shock to indicate the starting point of the fracture. The landward location of a main shock epicenter in its aftershock area suggests that there was higher potential for the rupture landward on the source area just before the main shock. Fukao (1977) suggested that a stress concentration could occur due to creep deformation on the boundary between an oceanic plate and a mantle beneath a continental crust in the vicinity of the seismic front. If a main shock is caused by the stress accumulation, it may be located on the landward side rather than on the seaward side, because the stress concentration may produce only weaker effects on the seaward. Several authors have reported preseismic slip corresponding to the above process. From the analysis of strain seismograms, Kanamori and Cipar (1974) suggested that a very large preseismic slip took place before the 1960 Chilean earthquake at the boundary between the subducting lithosphere and the asthenosphere on the downward extension of the main faulting. In northern Japan, Shimazaki (1974) showed that a rebound of the continental plate is due to a creep-like deformations at a deeper part of the interface between the two plates. Similar preseismic slip under different tectonic circumstances has also been reported by Thatcher (1975) and Fujii (1976). These preseismic deformations may be closely related to the driving force of plate motion. In regions subjected to normal subeuction, it is inferred that an oceanic lithosphere is dragged down by gravitational pull

of a denser sinking lithosphere (Isacks and Molnar, 1971 ; Abe, 1971). This may not be true, however, in regions of anomalous subduction such as New Georgia Island (No. 30) and the D'Entrecasteaux fracture zone (Nos. 6 and 29). In these regions, a stress concentration near the aseismic front may not occur at a preseismic stage. Under these situations, the main shocks Nos. 6, 29 and 30, would not take place under rule (1). In these cases, we will have to take into consideration a preseismic slip on the downward extension of the main shock fault.

The only report closely related to item (2) is the one by Imoto and Kishimoto (1977b), although some propagational patterns of aftershocks have been pointed out by Mogi (1968), Whitcomb *et al.* (1973), and Melosh (1976). Mogi (1968) reported rapid propagation of aftershock activities after the Alaskan earthquake of March 9, 1957 and March 28, 1964. In these cases, large aftershocks occurred along tne trenches within ten hours less after their main shocks, showing migrations at high speeds (one was about 60 km/h : the other 400 km/h). These migrations may not be the same as those referred to in this paper because of their high speed and their direction. Whitcomb *et al.* (1973) reported migrations of aftershocks at the speeds of 5~15 km/day at the time of the San Fernando earthquake of Feb. 9, 1971, which had a thrust type fault with some left-lateral strike-slip (Mikumo, 1973), but not in a subduction zone. Aftershocks with migrational features in this case occurred about a month after the main shock or later, and occupied only a small portion of the sequence.

Melosh (1976) has extended the work of Elsasser (1969) on stress propagation in the lithosphere to a model with a nonlinear viscous asthenosphere, and compared theoretical results with the seaward migration pattern of aftershocks for the Feb. 4, 1965, Rat Island earthquake (No. 5). Concerning the rheology of the asthenosphere, a viscoelastic model has also been proposed by Savage and Prescott (1978). In these models, they adoped tensile stress intead of shear stress as the criterion for aftershock occurrence. In the case when aftershocks occurred close to the seaward, they seem to be influenced more or less by tensile stresses, in accordance with the result of Stauder (1968). There are some differences between the migrations treated in this paper and in Melosh's (1976), in the location of aftershocks, their period of occurrence, focal mechanism and, most importantly, their pattern of migration. Although Melosh (1976) successfully explained the seaward migration pattern of the Rat Island sequence with his model, we will introduce a different model because of the above differences.

Ida (1974) proposed a model of slow-moving distubance to interpret migration of earthquakes and nonseismic creep. His model was based on the assumption that a thin fault gouge participates in viscous slip. Many researchers (Kasahara, 1975 ; Fujii, 1978 ; Thatcher and Rundle, 1979) attempted to interpret postseismic deformations as the results from afterslips on the faults. Among them, Thatcher and Rundle (1979) showed that the postseismic deformation of the 1946 Nankaido earthquake could be explained mainly by buried aseismic slip that occurred on the downward extension of the coseismic fault, and that contributions from asthenospheric relaxation were much smaller. There have been no reports that could provide a successful explanation to the pattern of aftershock activity by using an aseismic fault model. Since a postseismic deformation is one of the important after-effects of a large thrust earthquake in subduction zones and must have some relation to the activity of aftershocks, it may be impotant to take postseismic deformations into consideration. Here, we will abopt a fault gouge model in consistent with a buried slip model of Thatcher and

Rundle (1979).

Another approach might be possible in order to elucidate the process of **SSQA**. Through quantitative inspection, it has been found that **SSQA** represents regional variation of the decaying rate of aftershocks. Mogi (1963b) pointed out the similarity between the spatial distribution of regions with high decaying rates of aftershocks and that of regions with high heat flow anomalies. From experimental studies, Mogi (1962b) showed that the probability of fracture, $s(t)$, at the time t after the application of stress is represented by an exponential distribution, $s(t)=\mu e^{-\mu t}$, and that the rate μ is dependent on the stress as in $\mu=Ae^{\beta\sigma}$. But this result does not seem likely to be a key to **SSQA**, if the stational state of temperature and pressure is taken into consideration. For instance, there occurred two shocks Nos. 24 and 27 with a similar source process, which were close to each other in space and time; nevertheless, No. 27 shows **SSQA** and the other does not. In the Peru region without any volcanic line, **SSQA** is not recognized for the aftershock sequences Nos. 7 and 31. The presence of volcanoes, indicating the existence of melting zones or low viscous material, may play an importbnt role in the **SSQA**.

From the above discussions, our assumed fault gouge model must be built up to satisfy the following conditions.

(1) At the preseismic stage, a slip takes place on the downward extension of the main shock fault, which causes a stress concentration around the deeper end of the fault.

(2) At the postseismic stage, a buried slip also takes place mainly near the deeper end of the coseismic fault.

4.2 Criterion

When a certain initial displacement is given for the assumed fault gouge model, we can obtain time histories of the displacement and stress fields. To discuss the spatio-temporal pattern of aftershock sequences discovered in the preceding sections, a reasonable relation is required between these fields and the occurrence of aftershocks. For a preliminary estimation, here, we choose a shear stress working parallel to the gouge and its time-varing rate among three stress tensors in a two-dimensional model, considering the mechanisms of aftershocks (Stauder, 1968).

Ida (1974) gave a stress field (τ), in the case when a concentrated force is applied to $x=0$,

$$\tau=\frac{A\mu\nu t}{x^2+\nu^2t^2} \qquad (1)$$

ν has the dimension of velocity and is equal to $\mu w/2\eta(1-\nu_p)$, where μ, w, η and ν_p are the rigidity, thickness of the gouge, viscosity and Poisson's ratio, respectively, and x is taken parallel to the direction of the gouge.

Substituting $x=Ax$, $\nu t=At$ and $\tau=\mu\tau$ into the above equation, we have,

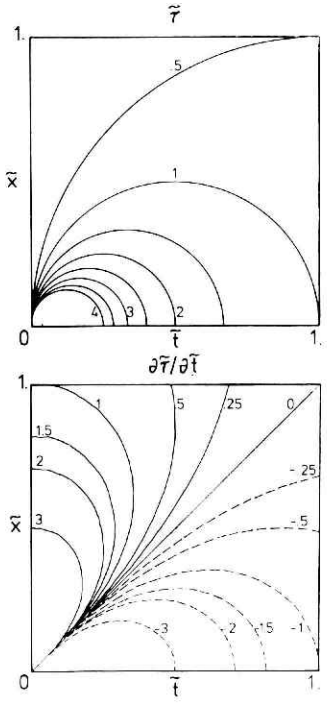

Fig. 21 Shear stress and its time derivative on the fault during viscous slip caused by concentrated force (see Ida, 1974). Contours indicate constant values of τ (upper) and $\partial\tau/\partial t$ (lower) as functions of x and t, where τ, x, and t are normalized variables. See the text for detailed description.

$$\tilde{\tau}=\frac{\tilde{t}}{\tilde{x}^2+\tilde{t}^2} \tag{2}$$

Differentiating $\tilde{\tau}$ with respect to $\tilde{t}$

$$\frac{\partial\tilde{\tau}}{\partial\tilde{t}}=\frac{\tilde{x}^2-\tilde{t}^2}{(\tilde{x}^2+\tilde{t}^2)^2} \tag{3}$$

Fig. 21 shows contours of $\tilde{\tau}$ (upper) and $\partial\tilde{\tau}/\partial\tilde{t}$ (lower) as functions of $\tilde{x}$ and $\tilde{t}$. If the number of aftershocks depends on stress level, the spatio-temporal pattern of aftershocks may be represented by the contours on the upper figure. On the contrary, if the frequency depends on stress rate, the pattern of aftershocks may be represented by those on the lower figure. Since the quiescent area starts at some point and spreads at a nealy constant speed, the latter case depending on the shear stress rate seems to be more explanatory of **SSQA** than the former case.

In these simplified expressions, however, it is not easy to identify the existence of a concentrated stress, and also the effects of a free surface near the fault are not included here. Therefore, by using a two-dimensional finite element methods, we will solve the stress fields from a more realistic fault model in a layered elastic structure with a free surface. The residual stress field just after a main shock and stress time histories will be calculated with appropriate initial conditions in the next chapter.

4.3 Residual stress field

The stress field at the postseismic stage may probably be closely related to aftershock occurrence, but the field has not been fully explored. For this reason, we will deduce the stress field just after a main shock from some related fields at preseismic and coseismic stages as follows.

At a preseismic stage, the stress will be built up near the fault of a coming main shock and its downward extension by a certain plate driving force. A preseismic slip may occur aseismically on its lower portion (a preseismic fault) to partially release the stress (Fig. 22, b). Consequently, this slip will cause stress concentration on the lower edge of the unslipped fault for a main shock, and then the resulted fracture will spread upward from there to the unslipped portion (Fig. 22, c). At this time, the displacement discontinuity on the preseismic fault remains preserved, since the main fracture ceases in a short time compared with the characteristic time of aseismic slip at the preseismic stage. The stress field right after this time may be regarded as the initial condition for a postseismic deformation. The postseismic slip could occur to decrease the residual stress over the whole length of the interface between the two plates (Fig. 22, d).

When the stress field around a thrust fault in a subduction zone is simulated by the finite ele-

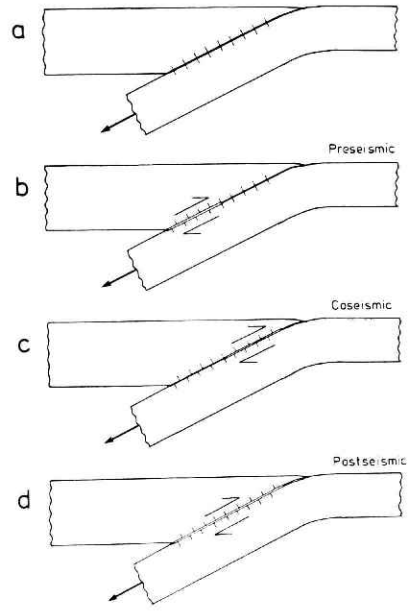

Fig. 22 Schematic figures of three stages. (b) : At the preseismic stage, a slip occurs on the lower part of the interface. (c) : At the coseismic stage, another slip occurs on the upper part of the interface and the rest of the interface maintains the discontinuity obtained at the preseismic stage. (d) : The viscous slip takes place over the whole area of the interface.

ment method, there are a few problems to be considered ; one is a driving mechanism, and the other is the distribution of slip on each of the preseismic and coseismic faults. The first problem is related to the boundary conditions for the model. The driving force of plate motion will be represented in terms of the force acting on a boundary. Isacks and Molnar (1971) showed an extensional stress field in the sinking lithosphere, on the basis of focal mechanisms of intermedite-depth earthquakes. Abe (1971) studied the focal process of a normal fault earthquake on March 30, 1965 beneath the Aleutian trench, and interpreted that gravitational pull exerted by the denser sinking lithosphere caused a large scale extensional fracture inside the oceanic lithosphere. Consequently, pulling force may be adopted as the boundary condition for the sinking lithosphere, on the basis of these prevailing hypotheses of subducting processes.

Regarding the second problem, we do not have sufficient data for the distribution of slip on a preseismic fault. For this reason, we prefer a simple distribution which satisfies the condition that the shear stress is completely released on the preseismic fault just before a main shock, rather than assume different types of complex distribution. We also assume in our model that at the coseismic stage the shear stress on the fault will be again completely released. However, this may not be true at both stages, and the residual stresses will tend to be smoothed out as time goes on. We will discuss the nonuniform field of residual stresses just after a main shock, but do not take these unreleased portions of stress ioto consideration here.

5. Stress analysis

5.1 Finite element method

Recently, the finite element method have often been used in seismological research to obtain displacement and stress fields (*e. g.*, Jungels and Frazier, 1973 ; Shimazaki, 1974a ; Miyashita and Matsu'ura, 1978). Since the method is a powerful analytical tool for simulating physical properties such as irregular geometry, heterogeneous properties, and so forth, it may be applied to investigate postseismic deformations in a subduction zone with complex geophysical structures where the oceanic plate underthrusts the continental plate with a shallow dip angle. For simulating residual stress during postseismic deformations, it is necessary to choose proper geometry, appropriate initial displacement discontinuity on the faults, boundary conditions, and heterogeneity of elastic constants. In this section, we will particularly treat with a fault gouge using a two-dimensional finite element method. Several related problems will be discussed in the following sections, and the results will be compared with the four observed cases which displayed **SSQA** most clearly.

The stress analysis in the finite element method (the displacement method) can be resolved into the following simultaneous equations,

$$[K]\ (U)\ =\ (F) \tag{4}$$

where vector U and F represent the nodal displacements and nodal forces respectively, and K is the stiffness matrix. It has been shown that a slight modification of this relation could simulate faulting process (Jungels and Frazier, 1973 ; Miyashita and Matsu'ura, 1978). We consider here the dislacement discontinuity on a fault surface which can be simulated by a sequence of double nodes bifurcated to either side. The displacement discontinuity (Δu_i) at the i-th pair of nodes is defined by

$$\Delta u_i = u_i^{(+)} - u_i^{(-)} \tag{5}$$

where $u_i^{(+)}$ and $u_i^{(-)}$ denote the displacement vectors at the upper and lower nodes, respectively. Substituting eq. (5) into (4), $u_i^{(+)}$ is eliminated. We assume the

Table 2 Examples of the conditions on fault. // and ⊥ indicate parallel and normal components to the faults, respectively

Component		Shear free	Dislocation	Friction
Δu_i	//	Unknown	Uo (known)	Unknown
	⊥	0	0	0
$u_i^{(-)}$	//	Unknown	Unknown	Unknown
	⊥	Unknown	Unknown	Unknown
$f_i^{(+)}$	//	0	Unknown	fo,i
	⊥	Unknown	Unknown	Unknown
$f_i^{(+)}+f_i^{(-)}$	//	0	0	0
	⊥	0	0	0

condition that a traction across the dislocation surface is continuous, that is,

$$f_i^{(+)} + f_i^{(-)} = 0 \tag{6}$$

where $f_i^{(+)}$ and $f_i^{(-)}$ are the traction acting on the upper-and lower- node of the i-th pair respectively. A transformation of the variable from (U, F, $u_i^{(+)}$, $u_i^{(-)}$, $f_i^{(+)}$, $f_i^{(-)}$) to (U, F, Δu_i, $u_i^{(-)}$, $f_i^{(+)}$, $f_i^{(+)} + f_i^{(-)}$) requires a transformation of the stiffness matrix from $[K]$ to $[K']$ symmetry of which is preserved. These transformations are performed for all pairs of nodes on the fault,

$$[K'] \begin{pmatrix} U \\ \Delta u_i \\ u_i^{(-)} \end{pmatrix} = \begin{pmatrix} F \\ f_i^{(+)} \\ f_i^{(+)}+f_i^{(-)} \end{pmatrix} \tag{7}$$

The conditions appropriate to a fault gouge for three cases are shown in Table 2. In the case of a viscous slip, $f_{o,i}$ is replaced by a viscous force, which is described as follows.

$$f_{oi} = c \frac{\partial \Delta u_{,,}}{\partial t} = c \Delta \dot{u}_{i,,} \tag{8}$$

where c is a function of viacosity, thickness of the gouge, and the grid spacing adopted. Eq. (7) is rewritten as follows,

$$[\mathrm{K'}] \begin{pmatrix} U \\ \Delta u_i \\ u_i^{(-)} \end{pmatrix} = \begin{pmatrix} F \\ f_i^{(+)}{}_{,,} = f_{oi} \\ f_i^{(+)}{}_{\perp} \\ f_i^{(+)} + f_i^{(-)} \end{pmatrix} = \begin{pmatrix} F \\ 0 \\ f_i^{(+)}{}_{\perp} \\ f_i^{(+)} + f_i^{(-)} \end{pmatrix} + [C]\ (\Delta \dot{u}_{i,,}) \tag{9}$$

$[C]$ is a diagonal matrix and has non-zero components only corresponding to slipping points. The slip rate ($\Delta \dot{u}_{i,,}$) can be approximated by the equation,

$$\Delta u_i(t) = \Delta u_i(t-\Delta t) + \{\Delta \dot{u}_i(t) + \Delta \dot{u}_i(t-\Delta t)\} \frac{\Delta t}{2} \tag{10}$$

where Δu_i and $\Delta \dot{u}_i$ are assumed to be a function of time and Δt is a time increment (Wilson and Clough, 1962). Substituting (10) into (9),

$$\left\{[K'] - \frac{\Delta t}{2}[C]\right\} \begin{pmatrix} U \\ \Delta u_i \\ u_i^{(-)} \end{pmatrix} = \begin{pmatrix} F \\ 0 \\ f_{i,}{}^{(+)}{}_{\perp} \\ f_i^{(+)} + f_i^{(-)} \end{pmatrix} - [C] \left\{\Delta \dot{u}_{i,,}(t-\Delta t) + \frac{2}{\Delta t} \Delta u_{i,,}(t-\Delta t)\right\} \tag{11}$$

Equations (10) and (11) give the time history of deformation at every time step.

Fig. 23 shows the finite element grid used in this study. It is assumed that there exists a fault running from point A to B where a sequence of the double nodes is traced. The assumed dip angle of about 27° ($\tan^{-1}0.5$) is an average one for those of large thrust earthquakes in subduction zones, say 15°~45°. The boundary of the continental block left of the fault is assumed to locate more distant than one fault length A-B away from the fault, but that of the seaward side is not. In calculating the stress field near the fault A-B, especially its upper portion, the boundary conditions on E-F-G are consider to have a sensitive effect on the results. To avoid these difficulties, the boundaries are usually set apart. In this case, however, another difficulty would arise out of the boundary F-G, and then we would have to take the material with different physical properties into consideration. We will discuss later these boundary conditions along B-G and F-G, in accordance with the regime of plate tectonics.

5.2 Initial conditions

In this section, we will examine the influence of initial values of displacement discontinuity which distribute over the fault A-B just after a coseismic slip. We deal with four different distribution of initial values, which result from two successional preseismic and coseismic slips. To make the effects of the initial values clear, elastic constants ($E=1.72\times10^{12}$ dyne/cm, Poisson's ratio, $\nu=0.25$) of material are assumed to be uniformly distributed over the whole region, and the boundary conditions, which are tabulated in Table 3, are used throughout all four cases. The preseismic deformation is assumed to be built up over such a long time range that we must consider the effects of the viscosity in the asthenosphere on the lithosphere through two boundaries D-B and F-G.

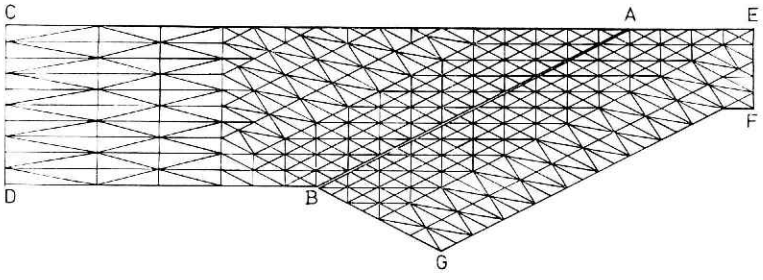

Fig. 23 Finite element grid.

These boundaries may be assumed to be a free surface, because the stresses out side D-B and F-G are considered to decrease due to creep deformation with a viscoelastic process. On the other hand, at the coseismic stage and also the postseismic stage considered here (within about ten days), the time scale of deformations is so short that the effects of viscosity of the asthenospheres would not have to be taken into consideration. In these cases, the asthenosphere may be treated as elastic material, with an overlaying free boundary (soft spring) or a fixed boundary (stiff spring). In this section, however, only the case of a fixed boundary is treated, and the alternative will be discessed in the next section.

In our model, within the limits of the scheme mentioned previously, the initial values of displacement discontinuities are related to the fault lengths at the preseismic and coseismic stages. Given the lengths of the faults at the two stages, the distribution of displacement discontinuities will be obtained uniquely because the shear stress is assumed to be completely released on the fault at each stage. The upper half of

Teble 3 Boundary conditions for cases **U** 1 ~ 4

Boundary Component		Preseismic	Coseismic	Postseismic
C-A-E	//	free surface	free surface	free surface
	⊥			
C-D	//	0-displacement	0-displacement	0-displacement
	⊥			
E-F	//	free surface	remain in their displaced position at preseismic deformation	
	⊥			
D-B	//	free surface		
	⊥			
F-G	//	free		
	⊥	0-displacement		
B-G	//	ΔU_0-displacement		
	⊥	free		
A-B	Pre-fault	shear free	—	viscous slip
	Out of Pre-fault	0-discontinuity		
	Co-fault	—	shear free	
	Out of Co-fault		hold their discontinuities at preseismic stage	

Fig. 24 indicates the fault extensions in four assumed cases **U**1~4, and the lower half shows the distributions of displacement discontinuity just after the coseismic stage. The unit of the ordinate corresponds to the displacement given on the boundary B-G.

Before comparing the results with observations, a few characteristics of the calculated stress patterns for all the models are described. Fig. 25 shows the distributions of shear stress as the results of preseismic (upper) and coseismic (lower) deformations respectively, in case **U**2. At the result of the preseismic deformation, shear stress decreses on the preseismic fault, while a stress concentration arises

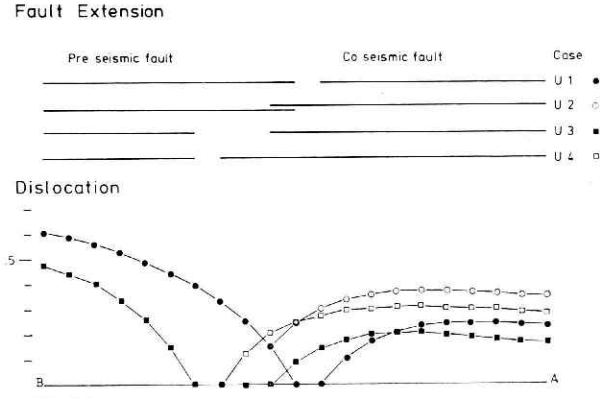

Fig. 24 Fault lengths of preseismic and coseismic stages and dislocation distribution just after the coseismic slip for cases **U**1~4. The unit of the ordinates in the lower figures is a given displacement (ΔU_0) at the lower end of the oceanic slab.

at its upper end. This deformation grows up until the concentrated stress satisfies a certain condition of the coseismic slip. At the coseismic stage, the faulting occurs so as to release the shear stress concentration at the previous stage. After the coseismic deformation, the stress concentration appears to shift downward to the end of the coseismic fault, with an intensity lower than that at the preseismic stage. A postseismic deformation will take place thereafter.

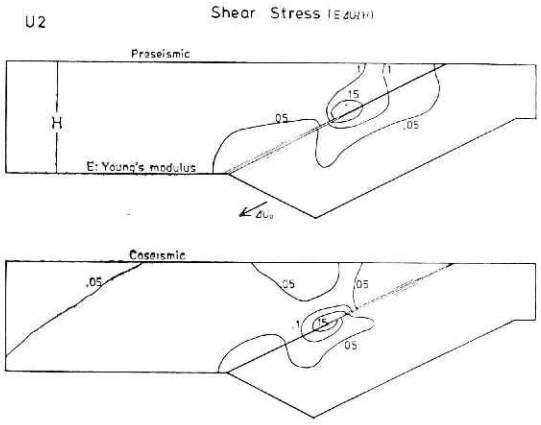

Fig. 25 Distributions of shear shess after the preseismic and coseismic slips in case **U2**. Each of the contours shows a constant value of stress (1 unit $=E\Delta U_0/H$).

Fig. 26 shows contours of the shear stress during postseismic deformation on the fault surface in the continental block, as functions of distance along the fault and time. It can be seen the figure that the stress concentrated at the central part in the previous stages remains longer than the initially lower stress at other position towards both end of the fault. Since these patterns of the contours are unlike the front of **SSQA**, it may be inferred that the shear stress itself can not be the critical level for aftershock occurrence, as has already been mentioned. Therefore, we will discuss the shear stress rate hereafter.

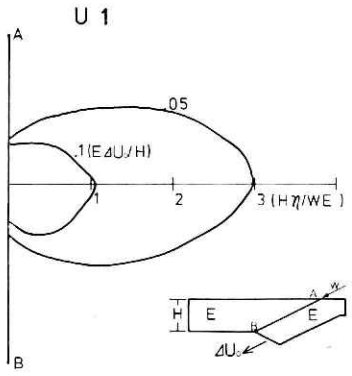

Fig. 26 Shear stress on the fault during postseismic deformation in case **U1**. The ordinate indicates the distance along fault AB and the abscissa is the time lapse after coseismic slip which is normalized by $H\eta/WE$. H, E, W and η are thickeess of the continental plate, young modulus, and thickness and viscosity of the gouge, respectively.

Fig. 27 shows comparisons of the stress releasing patterns during postseismic deformation among the four adopted models. Each contour indicates a transient time, which is defined here as the time when the shear stress takes a maximum value, and normalized by $H\eta/WE$ in the figure. Shaded zones indicate the areas where the shear stress increases just after the coseismic slip. It is found that the patterns of stress readjustment are generally similar in these four cases. The stress increasing area in each model is located at the upper and lower portion of the fault, and also at the area conjugate to them. The difference between the areas of the four models consistently corresponds to the difference between the coseismic fault lengths. Since aftershocks appear to occur nearly along coseismic faults in many cases, we will limit our discussion on the time history of the shear stress rate in the upper right shaded zone near the coseismic fault. In this zone, a transient time is longer at a seaward and upward point.

Next, the spatial distributions of the initial value of the stress increasing rate are presented. Each diagram in the upper part of Fig. 28 shows the initial stress

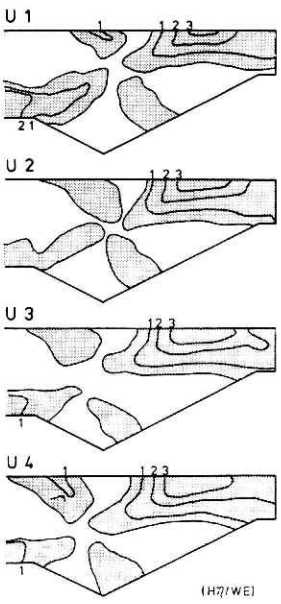

Fig. 27 Transient time for cases U1~4. The shaded areas of each set indicate the increase in stress after coseismic slip. Contours show constant values of transient time when the shear stress takes a maximum value at each point (unit=$H\eta/WE$).

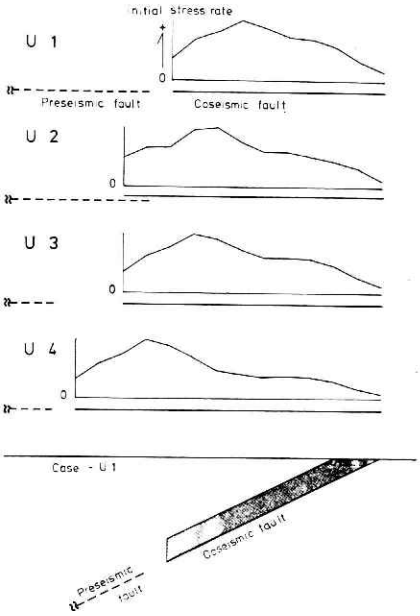

Fig. 28 Initial distributions of the stress increasing rate for cases U1~4. Each set of the upper four diagrams shows distribution of stress increasing near the coseismic fault. The curve is drawn in relation to the positions of the preseismic (broken line) and coseismic (solid line) faults. For the sake of calculation, the stresses on the fault and above it (0.1 H) are averaged (shaded area of the bottom in case U1).

rate (folded line) distributed at different positions on the preseismic (broken line) and coseismic (solid line) faults. The initial rate here represents a summing up of the positive rate within a thickness of one tenth of H above the coseismic fault (the shaded zone in the bottom figure for case U1), and is normalized by the maximum value in each set. Although the distributions in the four cases appear similar to each other, the position for the maximum is slightly different between the four cases, which may be due again to the difference between the fault lengths.

In later sections, we will choose a suitable model among the above four mndels in order to explain migration of actual aftershock sequences, by comparing the position of the maximum stress rate with the most active area of aftershocks on a coseismic fault.

5.3 Boundary conditions

The effects of the boundary conditions adopted here will be discussed on the basis of the results from two different cases B1 and B3. Elastic constants in these cases are the same as those of models U1~4, and this fault lengths of the preseismic and coseismic stages are taken as the same as those of U1 and U3, respectively, so

that we can discuss only the effects of boundary conditions.

The boundary conditions in case **B3** are tabulated in Table 4. In this case, boundaries D-B and F-G are kept free throughout the three successive seismic stages,

Table 4 Boundary conditions for case **B 3**

Boundary	Component	Preseismic	Coseismic	Postseismie
C-A-E	//	free surface	free surface	free surface
	⊥			
C-D	//	0-displacement	0-displacement	0-displacement
	⊥			
E-F	//	free surface	same as preseismic	
	⊥			
D-B	//	free surface		
	⊥			
F-G	//	free		
	⊥	0-displacement		
B-G	//	ΔU_0-displacement	remain in displaced position at preseismic deformation	
	⊥	free	free	free
A-B	Pre-fault	shear free	—	viscous slip
	Out of Pre-fault	0-discontinuity		
	Co-fault	—	shear free	
	Out of Co-fault		hold their discontinuities at preseismic stage	

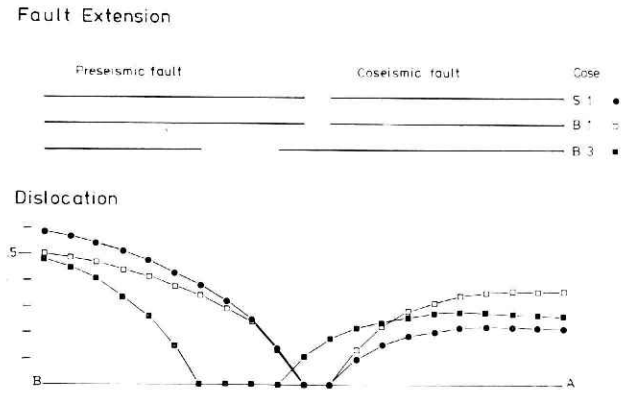

Fig. 29 Preseismic and coseismic fault lengths and their dislocation distribution just after coseismic slip for cases **S1**, **B1**, and **B3**.

except for the normal component on the boundary F-G. These conditions with free boundaries (soft spring) may become cases imposed on an elastic asthenosphere, and are completely different from the fixed boundaries (stiff spring) assumed in case **U3**. Fig. 29 shows the fault lengths assigned for three different cases and corresponding distribution of displacement discontinuity just after a coseismic slip. The displacement discontinuities in case **B3** along the coseismic

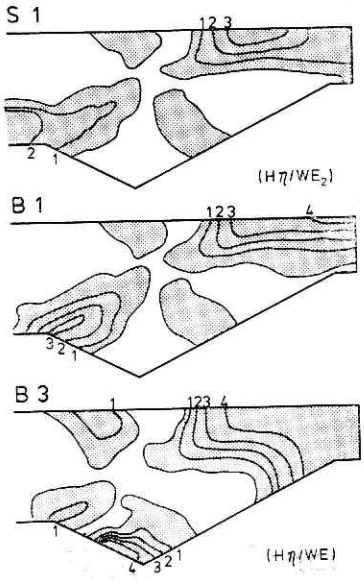

Fig. 30 Transient time for cases S1, B1, and B3. See Fig. 27 for notation. $N.B.$ the time unit (1 unit$=H\eta/WE_2$) for the case S1.

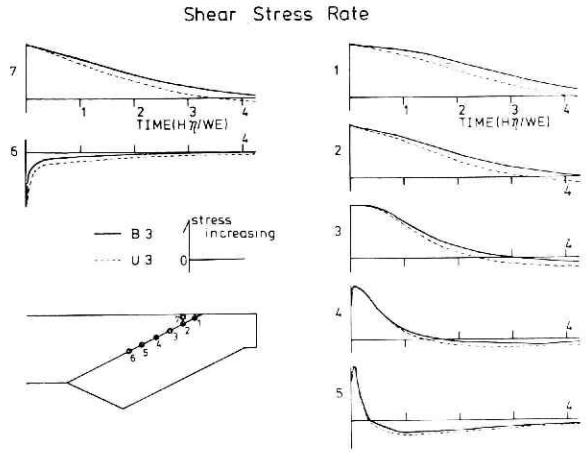

Fig. 31 Vatiations in shear stress rates with time at several points. The curves of variation for case **B3** (solid line) are compared with those for case **U3** (broken line).

fault are larger than those in case **U3**, as understood from comparison between Figs. 24 and 29.

The bottom of Fig. 30 shows contours of the transient time in case **B3**. It is noticed that there are several differences between cases **B3** and **U3** in the shapes of contours along the bottom of the down-going slab, that is, its down warping in the upper portion and concentration in the lower portion. Also, the transient times in case **B3** near the coseismic fault are longer than those in case **U3**, which seem worth considering for the study of aftershock occurrence.

Fig. 31 shows time variations of the shear stress rate at several selected points along the fault. Solid and broken curves indicate those in cases **B3** and **U3**, respectively, which are normalized by the respective maximum value at each of the points. The ratio of the normalization factor in case **B3** to that in case **U3** differs from point to point within the range of 1.14~1.20. These variations within 5% do not seem to be serious at this stage of the present study. Immediately near the points of stress concentration, point No. 6, shear stress decreases vary rapidly at the initial stage, and later more slowly. In the other locations, the shear stresses increase initially and later gradually decrease. The transient time when the stress rate changes from the increasing state into a decreasing one seems merely proportional to the distance from the point of stress concentration. See solid curves for case **B3** are similar to those of **U3**, but the difference in the transient time between the two curves becomes larger in proportion to the distance. The differences between the transient times in the two cases are within 20%. It may be concluded that the differencc in the boundary conditions between cases **B3** and **U3** yields a difference of the order of 10~20% in the estimated time constant or viscosity of material.

Next, we will discuss one more case **B1** with different boundary conditions, which are tabulated in Table 5. The boundary conditions applied to F-G are assumed here to be a convectional force acting on the bottom of the down-going slab. The

Table 5 Boundary conditions for case **B1**.

Boundary	Component	Preseismic	Coseismic	Postseismic
C-A-E	//	free surface	free surface	free surface
	⊥			
C-D	//	0-displacement	0-displacement	0-displacement
	⊥			
E-F	//	free surface	same as preseismic	
	⊥			
D-B	//	free surface		
	⊥			
F-G	//	ΔU_0-displacement	remain in displaced position at preseismic deformation	
	⊥	0-displacement		
B-G	//	free surface	free surface	free surface
	⊥			
A-B	Pre-fault	shear free	—	viscous slip
	Out of Pre-fault	0-discontinuity		
	Co-fault	—	shear free	
	Out of Co-fault		hold their discontinuities at preseismic stage	

locations of preseismic and coseismic faults and the distribution of displacement discontinuities are again displayed in Fig. 29. It is to be mentioned that the displacement discontinuities near the surface are larger than those in any other cases due to the convectional force. The middle of Fig. 30 shows contours of the transient time in this case, which do not seem very different from that of case **U1** near the coseismic fault. This situation is also clear in Fig. 32, where time variations of the shear stress rate along the coseismic fault are shown. The differences between the solid curves (case **B1**) and broken curves (case **U1**) are more

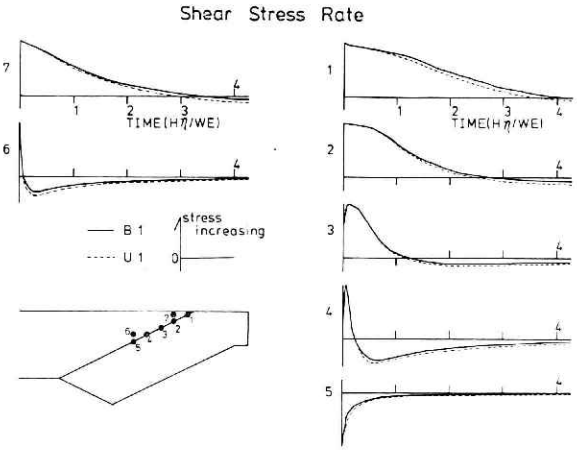

Fig. 32 Variations of shear stress rate with time at several points. The curves of variation for case **B1** (solid line) are compared with those for case **U1** (broken line).

slight than those between cases **B3** and **U3**. The ratios of the shear stress rate in case **B1** to those in case **U1** are within the range of 1.13~1.29, which are somewhat larger than that between cases **U3** and **B3**.

The results of comparison between two cases with different boundary conditions, indicate that the pattern of time variation of shear stress rates is not seriously influenced qualitatively by the boundary conditions imposed on the bottom of the slab. Quantitatively, however, the maximum shear stress rate is somewhat different from case to case, although the ratios in their maxima between two corresponding cases (**B3** and **U3**, **B1** and **U1**) are nearly constant within about 5%.

5.4 Velocity structure

It is one advantage of the finite element method that complex geometries and heterogeneities can be easily simulated. With this advantage, we will discuss the effect of a layered structure of seismic wave velocities. The velocity structure in a subduction zone is very complex, and various models have been proposed by many researchers (Kanamori, 1970c ; Grow, 1973 ; R.G.E.S., 1977). Since a simple layered model may be enough to estimate the influence originating from a velocity structure, case S1, with a simple structure, will be examined in this section.

Table 6 represents the structure of elastic constants which is referred to several already reported velocity models. For the sake of comparison, the same simulation is made for case **S1** as in the case of **U1**. The locations of preseismic and coseismic faults and the distribution of displacement discontinuities are again displayed in Fig. 29. The top of Fig. 30 shows contours of the transient time in case **S1**. For convenience of comparison, elastic constants of the lower layer of the continetal side (E_2, ν_2) are taken equal to those of case **U1** (E, ν). The contours in case **S1** appear quite similar to those in case **U1** except for the portion near the surface, but the transient time in case **S1** at points near the surface is somewhat longer than that of **U1**. This difference can be seen more clearly in Fig. 33, which shows time variations of the shear stress rate at several selected points along the coseismic fault. The curves at points Nos. 4, 5 and 6 in the lower layer fairly well agree with those in case **U1** (broken line), while those at points Nos. 1, 2 and 7 in the upper layer are longer than those in case **U1**. These differences come from the difference in the characteristic times, $H\eta/WE$, $H\eta/WE_1$ and $H\eta/WE_2$. The ratios of the normal-

Table 6 Elastic constants of case **S1**.

	Depth	E 10^{12} dyne/cm^2	ν	V_p km/sec	V_s km/sec
Continental Block	0 -0.3H	1.009	0.271	6.6	3.7
	0.3-1.0H	1.723	0.251	7.8	4.5
Oceanic Block	0 -1.0H	1.996	0.255	8.2	4.7

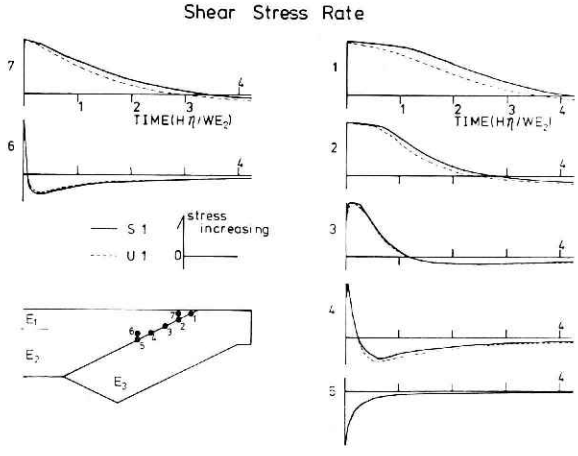

Fig. 33 Variations of shear stress rate with time at several points. The curves of variation for case **S1** (solid line) are compared with those for case **U1** (broken line).

ization factors in case **S1** to those in case **U1** scatter in the range of 1.14～2.12, indicating larger value in the lower layer than those in the upper layer. In this sense, the influence of the layered structure is not negligible. An introduction of the layered structure might improve the fitness between the observed data and the calculated results. In this study, however, we implicitly consider another factor, the fracture strength. For the uniform model, we can simply assume the uniformity of strength, which is not well known at this point. Therefore, we will use a uniform model at the time of comparison with the observed data in the next section.

5.5 Comparisons with observed data

In this section, we will show the results of comparisons with the observed sequences, Nos. 2, 18 and 19, and the superposed data of the Kurile sequences (Nos. 1, 11, 16 and 28). These are the aftershock sequences that took place in various regions of typical subduction zones and showed **SSQA** clearly, as have been mentioned previously. We will compare the spatio-temporal patterns of these sequences wite the results of numerical simulations. From four cases **U1**～4, one case will be seleted for each sequence, but the other cases (**B1**, **B3** and **S1**) are not considered here because of the reasons given in the previous sections. We assume that the rate of stress increase is proportional to the density of aftershock occurrence and that aftershocks could not occur at a certain point when stress decreases there. With these assumptions, **SSQA** can be expected to occur in accordance qualitatively with the stress rate as shown in Figs. 31, 32 and 33. Now we describe some results of quantitative comparisons as follows.

The Alaskan sequence of May 28, 1964 (No. 2) : This sequence consists of a large number of shocks, but the front of the quiescent area is not so clear. However, these shocks offer stable decaying curves of frequency at each point as shown in Fig. 18. The initial values for the curves in Fig. 18, $P(x, 0)$ which is the normalization factor at each point, and their expected values are indicated by the symbols of closed circles and open circles, respectively in Fig. 34. Case $U4$ is adopted for this comparison because of the following reason. We can estimate from Figs. 3 and 34 that the distances

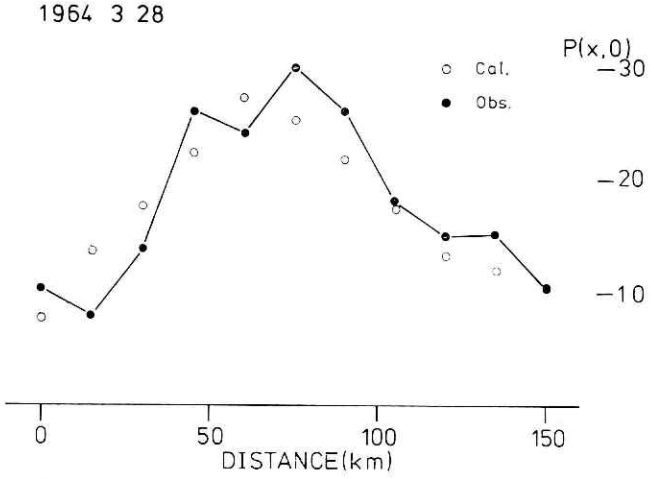

Fig. 34 Spatial distribution of aftershocks just after the Alaskan earthquake, and the expected distribution from case **U4**. Closed circles indicate initial frequencies defined by the smoothing method (see the text). Open circles show the stress increasing rate at the initial time, and the total of open circles is equalized to that of closed circles.

from the landward side of the aftershock area to the trench axis, and to the most frequent area of aftershocks just after the main shock, are about 250 km and about 60 km, respectively. Thus the former is about a quarter of the distance from the landward side. The spatial distribution of the initial rate in case *U4* (Fig. 28) shows the maximum at the similar position, which is located about a quarter of the coseismic fault away from its landward end. The total number of the expected values at all points in Fig. 34 is equalized to that of the observations. This equalization gives a conversion factor from a stress increasing rate to a density of aftershock occurrence.

Next, the frequency decay curves for this earthquake sequence, $P(x, t)$ are compared with their expected curves (solid) in Fig. 35. Dotted curves are taken from Fig. 18, each of which is normalized by its initial value. We may estimate a viscosity in such a way that the expected curves can be best fitted to the observed curves by a visual inspection. The fitness of the two curves at each point is not really satisfactory, however, the regional tendency of their decaying rate appears to agree to a reasonable extent.

The superposition of southern Kurile sequences : The superposed deta of the southern Kurile sequences which were used in the section 3.3 are compared with case *U2*. The procedures are the same as in the case of the Alaskan sequence. Fig. 36 shows the spatial distribution of the initial values of decaying curves, $P(x, 0)$ and their expected values from the model. Fig. 37 shows the frequency decay curves of the superposed sequences (dotted ; see Fig. 20)

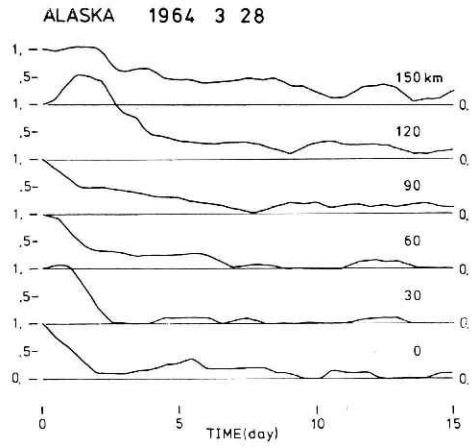

Fig. 35 A comparison of frequency decaying curves between the **U4** and the Alaskan sequence. Solid and dotted curves indicate frequency decaying curves at every 30 km distant from the main shock normal to the trench obtained by the simulation of case **U4**, and by the smoothing method for the Alaskan sequence. Each curve is normalized by its initial value. Dotted curves are the same as those of Fig. 18.

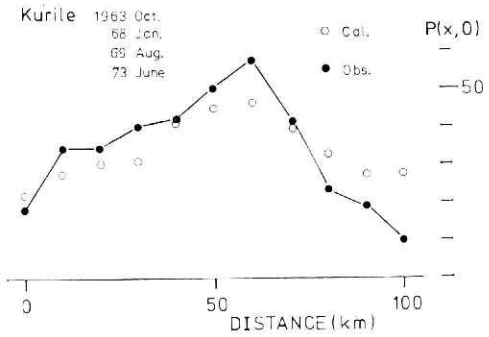

Fig. 36 Same as Fig. 34 but for case **U2** and for the superposed data of four sequences in the Kurile region.

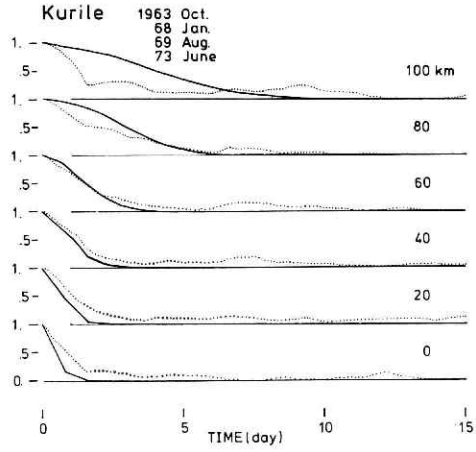

Fig. 37 Same as Fig. 35 but for case **U2** and for the superposed data of four sequences in the Kurile region.

and their expected values (solid). Agreement between the two curves appears satisfactory except for those at a 100 km distance. It is also noticed in Fig. 36 that there is a difference in the initial frequency between the superposed data and the calculated results at this distance, and that the former values are about one third of the latter. This evidence seems to imply that the extent of aftershock area toward the oceanic side is less than 100 km.

In the above two cases, we have been able to obtain smooth curves of frequency decay at every point. On the contrary, the other sequences except for No. 5, the Rat Island sequence of Feb. 4, 1965, do not have enough aftershocks to obtain this type of curves. For these sequences we will compare the time variation of the expected frequency with the observed data by some modified procedures. These procedures will be applied to two sequences, Nos. 18 and 19.

The sequence of April 29, 1970 (No. 18) in Middle America : This sequence shows clear **SSQA** and it is easy to note that the front of the quiescence reaches the seaward side of the aftershock area six or seven days after the main shock (see Fig. 11). Fig. 38 shows the spatial distribution of the observed aftershocks (closed symbols) and the expected results (open symbols) during periods of six days (squares), and the first half day (circles). Case *U4* is adopted for comparison with this sequence. The expected frequency in case *U4* during the period just after the coseismic slip to the transient time is most similar to the spatial distribution of the aftershocks observed during the first six days on the extension from the lnndward side to the trench axis. In this figure, closed symbols (observation) indicate the number of shocks averaged over those within ±15 km, and for open symbols (calculation), a similar running means technique is operated. The total expected number during the six days (open square) is equalized to that of the observed data (closed square). From these comparisons, we obtain the conversion factor from a stress increasing rate to a density of aftershock occurrence. Using this conversion factor, we derive the corresponding distribution during the first half day (open circle).

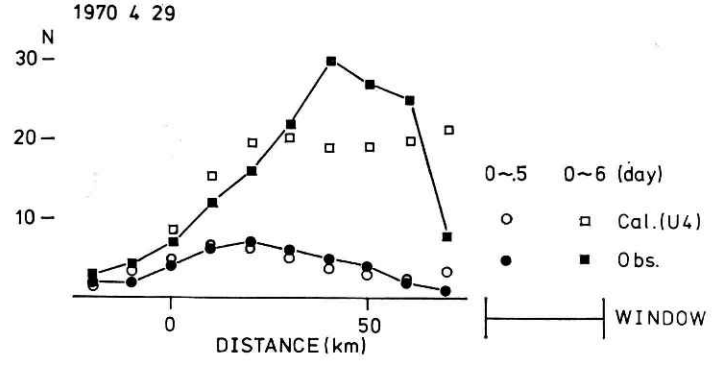

Fig. 38 Spatial distribution of the observed sequence of Apr. 29, 1970, and the expected sequence. Closed symbols (observation) indicate the number of shocks within a +15 km distance and open symbols are those of simulation for case U4. The total number of open squares is equalized to that of closed squares (observation). Using this converting factor between data and simulation, the expected distribution during the first half day (open circle) is calculated.

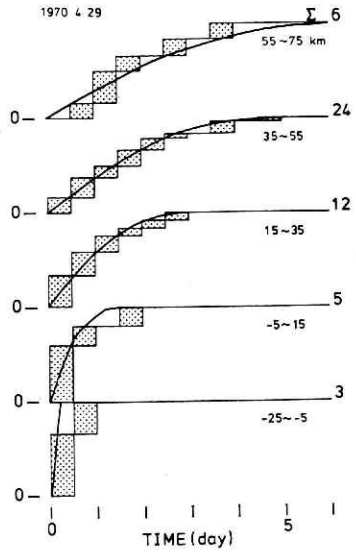

Fig. 39 Cumulative histograms of shocks of the sequence of Apr. 29, 1970, and expected curves. Dotted blocks show the number of shocks for every half day within each range of distance. The numbers on the upper right of each set are the total number in each range, and the distances from the main shock normal to the trench. Each calculated curve is equalized to each total number.

Table 7 Viscosities for the sequences showing **SSQA**.

No.	Date	Viscosity (x 10^{15}poise)	Remarks
1	1963 Oct. 13	3.5	see section 5.5
2	1964 Mar. 28	4.5	see section 5.5
3	1964 July. 24	3.5	refer to Nos. 1, 11, 16 and 28
5	1965 Feb. 4	4.4	—
6	1965 Aug. 11	6.	—
8	1966 Dec. 28	6.	refer to No. 19
9	1967 Oct. 4	6.	refer to No. 20
11	1968 Jan. 29	3.5	see section 5.5
12	1968 May. 16	4.5	—
13	1968 May. 20	10.	—
16	1969 Aug. 11	3.5	see section 5.5
18	1970 Apr. 29	3.	see section 5.5
19	1971 July. 9	6.	see section 5.5
20	1971 July. 14	6.	—
21	1971 July. 26	4.5	—
22	1971 Dec. 15	4.5	—
26	1972 Dec. 2	6.	—
27	1972 Dec. 4	6.	—
28	1973 June. 17	3.5	see section 5.5

Next we examine the time variation of frequency in each subdivision of the aftershock area. Fig. 39 shows a cumulative number of shocks that occurred during every half day (dotted block) in each subarea with a 20 km width, and the corresponding integrated number of calculations (solid curve). The final value of each curve is equalized to the total number (upper right) in each subarea. The viscosity of fault gouges may be estimated also from the curves which can be fitted to the cumulative histograms. It may be concluded for this sequence that the agreement between the observed data and expected values in time and space are satisfactory. The viscosity estimated from these curves is given in Table 7, where the thickness of fault gouges is 1 km.

The sequence of July 9, 1971 (No. 19) in Chile : This sequence also shows clear **SSQA**. Comparisons between the observations and calculations can be given in the same way as the previous case. Figs. 40 and 41 show the spatial distribution of this sequence and its time variation in different subareas. Except for the bottom set in Fig. 41, the calculated curves satisfactorily agree with observation in space and time. The bottom set shows much longer duration of aftershock occurrence than that expected. Any other possible model could not explain this long duration near the landward side.

Comparisons for several other sequences with **SSQA** are shown in Appendix 2, corresponding to Figs. 39 and 41. From these results, it may be concluded that the spatio-temporal patterns of aftershocks with **SSQA** can be explained by a rather simple fault gouge model with a simple stress increasing rate. The above successful results are based on a three-stage model, stress concentration on the fault and the stress

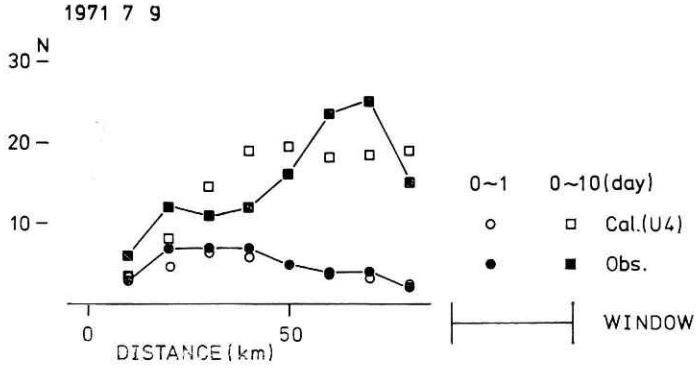

Fig. 40 Same as Fig. 38 but for the sequence of July 9, 1971.

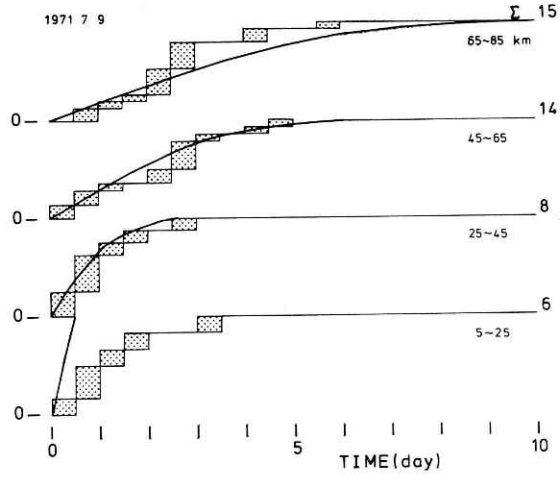

Fig. 41 Same as Fig. 39 but for the sequence of July 9, 1971.

increasing rate for aftershock occurrence. Detailed discussion on these problems will be made further in the next chapter.

6. Discussion

6.1 Preseismic and postseismic slips

Dislocations at preseismic and postseismic stages : We have built up our model of aftershock occurrence by focussing attention to elucidate **SSQA** ; the results appear reasonably satisfactory. On the other hand, the observed crustal deformations which may be caused by preseismic or postseismic slips have not been quantitatively discussed in the foregoing sections. Our models will be examined from a view point of crustal deformation.

Table 8 summarizes several parameters of preseismic, coseismic and postseismic slips in subduction zones, which have been estimated by several researchers, together with those derived from our simulation in case **U2**. Only one case of preseismic slip was observed about 15 minutes before the Chilean earthquake (Kanamori and Cipar, 1974), in which the moment and average dislocation have been estimated about one

Table 8 Comparisons of dislocations at three stages.

Event	Stage	L km	W km	D_o m	M_o dyne/cm^2	T	Reference
Chile	Preseismic	800	200	30 20	3.5×10^{30}	300-600s	Kanamori and Cipar, 1974 Okada, 1980
1960 May 20	Coseismic	300	200	24	2.7×10^{30}		Kanamori and Cipar, 1974
Tonankai	Coseismic	120	80	3.1	1.5×10^{28}		Kanamori, 1972
1944 Dec. 7	Postseismic	80	80	2.5	4.8×10^{27}	4 yr	Fujii, 1976
Nankai	Coseismic	120	80	3.1	1.5×10^{28}		Kanamori, 1972
1946 Dec. 20	Postseismic	65 150	15 30	2.5 2.5	7.3×10^{26}	4 yr	Yamada and Kashara, 1975 Thatcher and Rundle, 1979
Tokachi	Coseismic	130	100	2.45			Fujii, 1979
1952 Mar. 4	Postseismic	130	60	0.2			Fujii, 1979

Model	Stage	$L/\overline{AB}$	$D/\overline{\Delta U_o}$	$L/\overline{AB}\cdot D/\overline{\Delta U_o}$
U 1	Preseismic	0.5	0.43	0.22
	Coseismic	0.45	0.21	0.1
	Postseismic	0.2	0.3-0.4	0.06-0.08

third larger than those of the main shock. More recent study by Okada (1980) gives a 1/2~2/3 times smaller moment and dislocation for this precursory slip than that of Kanamori and Cipar (1974). Contrary to these observed data, as seen in the table, the average dislocation ($D/\overline{\Delta U_o}$) and the product of the fault length and dislocation at preseismic slips ($L/\overline{AB}\cdot D/\overline{\Delta U_o}$) are two times larger than those at the coseismic stage in case **U1**. However, these discrepancies do not seem to be very large, in view of our two-dimensional simulations, in which the driving force of the oceanic plate has been applied to its lower end, yielding the preseismic slip and successive deformations.

For the observations of postseismic deformations given in the table, the average dislocation and moment are 0.1~0.8 and 0.05~0.3 times smaller than those of coseismic slips, respectively, whereas case **U1** gives 1.5~2. and 0.6~0.8 for the corresponding ratios. If these observed parameters give normal relations between preseismic, coseismic and postseismic slips, our model may have overestimated postseismic deformation. To reconcile these discrepancies, other processes before postseismic deformations would probablv be required. Even with a small postseismic deformation, however, if high stress concentration alreadv existed at the lower end of the coseismic fault, **SSQA** could take place. An emergence of **SSQA** depende critically on a residual stress pattern rather than the residual stress level itself.

Characteristic time of after-effect : There are many reports on postseismic deformations after several past large earthquakes. Related to the sequences in this paper, Tada (1974a,b) and Kasahara (1975) reported postseismic deformations following the Nemuro-Oki earthqake of June 17, 1973. Tada (1974a,b) shows transitional upheaval at Hanasaki during a period of about 10 days after the shock with the differences in daily mean sea level between the Hanasaki and Kushiro tidal observatories (lower right of Fig. 42). On the other hand, Kasahara (1975) proposed a retarded faulting

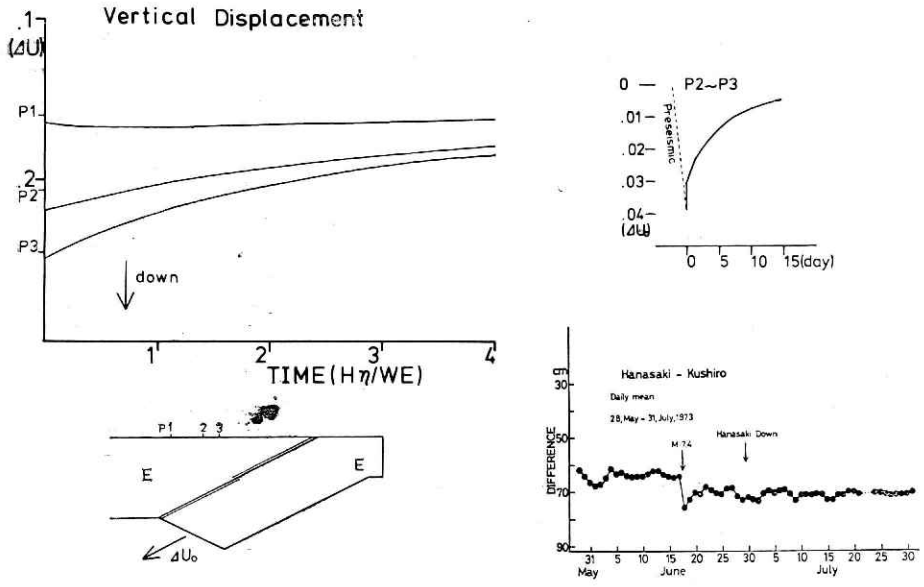

Fig. 42 Examples of vertical displacement. Time variations of vertical displacement at a few points are shown for case **U4** (upper left). The time variation of difference between two points is shown (upper right). The time constant is the same as that of Fig. 37 so as to compare with observed data (lower right). The observed data indicate the differences in daily mean sea level between the Hanasaki and Kushiro tidal observatories (see Tada, 1974a).

on a down-ward extension of the main shock fault. The monthly mean data of tidal difference between Hanasaki and Urakawa were used in his paper, which indicate upheaval at Hanasaki for about 2 years after the shock. This duration was ascertained later by Kato and Tsumura (1979). There is a considerable difference in time constants between the two authors, that is, about 10 days (Tada) and 2 years (Kato and Tsumura) (8 years in Kasahara's paper (1975)). The upper left and right hand-sides of Fig. 42 show the calculated vertical displacement for case **U2** at a few points on the surface, and their difference between two points, **P2** and **P3**, respectively. It can be seen that the upper right figure explains well the transitional upheaval data shown in the lower right figure (Tada, 1974 a,b). The left figure appears to have a slightly longer time constant than that of the right (time=4 corresponds to 15 days), but this difference seem too small to account for the great difference between the time constants. Our model would not able to explain the deformation with the longer time constant given by Kato and Tsumura (1979). It may be necessary to consider another process for postseismic deformation with a long duration time.

6.2 Frequency decay law

The frequency decay law of aftershocks, which is well represented by the Omori's (or modified Omori's) formula, is one of the well known propeties of aftershock phenomena. Most theories of aftershocks have attempted to explain this formula. Our model successfully explained spatio-temporal pattens of aftershock activities during a period of about 10 days, and the consistency with frequency decaying needs not be discussed again. However, for further study of aftershocks, some related problems

will be dicussed.

Analytical derivation of the Omori's formula: For the analytic and basic discussion on the frequency decay law, we refer again to Ida's paper (1974). The initial condition on the fault may be given by a δ-function of displacement discontinuty, because any complex function can be represented by integration of a δ-function. The deformation of the SH mode is solved. The discontinuity on the fault is represented by

$$D=-\frac{\tilde{t}}{\tilde{x}^2+\tilde{t}^2} \tag{12}$$

which is derived by the inverse Fourier transform of equation (8) in his paper. For D, $\tilde{t}$ and $\tilde{x}$, see setion 4. 2. Shear stress $\tilde{\tau}$ in the region of $\tilde{x}$, $\tilde{y}>0$ is given by

$$\tilde{\tau}=-c\,\frac{\tilde{x}^2-(\tilde{y}+\tilde{t})^2}{\{\tilde{x}^2+(\tilde{y}+\tilde{t})^2\}^2} \tag{13}$$

where $\tilde{y}$ represents the distance from the gougeand c is a constant. Differentiating $\tilde{\tau}$ with respect to $\tilde{t}$,

$$\frac{\partial\tilde{\tau}}{\partial\tilde{t}}=-\frac{2c(\tilde{y}+\tilde{t})(\sqrt{3}\,\tilde{x}-\tilde{y}-\tilde{t})(\sqrt{3}\,\tilde{x}+\tilde{y}+\tilde{t})}{\{\tilde{x}^2+(\tilde{y}+\tilde{t})^2\}^3} \tag{14}$$

$\partial\tilde{\tau}/\partial\tilde{t}$ is positive if $\tilde{y}$, $\tilde{t}>0$ and $\sqrt{3}\,\tilde{x}-\tilde{y}-\tilde{t}<0$. It is understood from the above equation that the spreading velocity of a quiescent aftershock area corresponds to the condition given by $\sqrt{3}\,\tilde{x}-\tilde{y}-\tilde{t}=0$.

Under the criterion that the probability density of aftershock occurrence in any area is proportional to the stress increasing rate there, the density $\rho(\tilde{t},\ \tilde{x},\ \tilde{y})$ is given by

$$\rho(\tilde{t},\ \tilde{x},\ \tilde{y})=\begin{cases}\partial\tilde{\tau}/\partial\tilde{t} & (\partial\tilde{\tau}/\partial\tilde{t}\geqq 0)\\ 0 & (\partial\tilde{\tau}/\partial\tilde{t}<0)\end{cases} \tag{15}$$

Integrating $\rho(\tilde{t},\ \tilde{x},\ \tilde{y})$ with respect to $\tilde{x}$ and $\tilde{y}$, we obtain total frequency, $\mu(\tilde{t})$, over the whole region,

$$\mu(\tilde{t})=\int_0^\infty\int_0^\infty \rho(\tilde{t},\ \tilde{x},\ \tilde{y})\,d\tilde{x}d\tilde{y}=c\int_{\tilde{t}/\sqrt{3}}^\infty\left[\frac{1}{8\tilde{x}^2}+\frac{\tilde{x}^2-\tilde{t}^2}{(\tilde{x}^2+\tilde{t}^2)^2}\right]d\tilde{x} \tag{16}$$

Substituting $u=\tilde{x}/\tilde{t}$

$$\mu(\tilde{t})=c\,\frac{1}{\tilde{t}}\int_{1/\sqrt{3}}^\infty\left[\frac{1}{8u^2}+\frac{u^2-1}{(u^2+1)^2}\right]du \tag{17}$$

$\mu(\tilde{t})$ represents the Omori's formula. The integral of the above equation converges to a constants. From these consideration it seems that the law can be derived essentially from the combination of the viscous gouge model with a proper initial condition and the criterion used in this study.

After the main shock, stress concentrations will probably appear on and around many unslipped portions on the fault. In cases showing clear **SSQA**, however, one high stress concentration appears to have controlled aftershock occurrence, in view of the above derived inverse power law corresponding to the stress increasing rate. In other cases, it is possible for many distributed concentrations with comparable size to affect aftershock occurrence more or less. In the latter cases, a modified Omori's formula will be derived by summing up each inverse law corresponding to the individual concentration.

Frequency decay in the finite element model: It has been shown that our realistic model provides a successful explanation to **SSQA**. The phenomena of **SSQA**

appear for about 10 days or so after the main shock. After **SSQA**, there still remains minor aftershock activity, which is at most one tenth of that occurring during **SSQA**. In the previous chapter, such minor activity has been neglected, because we could not explain it with our model. Now, we make an attempt here to extend the conception of our model, in order to explain this later activity.

The lower solid curve of Fig. 43 should correspond to the frequency decay of aftershocks, which is derived from summing up the shear stress increasing rate on and near the coseimic fault (shaded portion of Fig. 43). The broken curve is a logarithmic decay curve given by $A \cdot \log(t+0.2)$ for reference. After time=1, the difference between the two curves becomes noticeable and reaches ten times at about time=4, suggesting that the solid curve can no longer be represented by a modified Omori's formula. Although not shown here, this difference could not be reconciled, if we take a wider region with a shaded zone in the upper figure for consideration. On the other hand, the upper curve of Fig. 43 also shows a frequency decay curve based on an extended conception that an aftershock occurs in regions where elastic potential energy is increasing. The curve has been derived from total energy increase at each triangular element in the shaded zone. The decaying rate of this curve is slightly lower than 1 in the early stage and is nearly equal to 1 in the later. This may be because the increase in energy comes from the increase in shear stress of not only the parallel component to the fault but also that of the other direction, whereas the lower solid curve indicates the increase in shear stress of only the parallel component. The difference between the two solid curves the increase in shear stress in other directional components at a later time, suggesting the possibility of aftershock occurrence with different focal mechanisms occurring after **SSQA**.

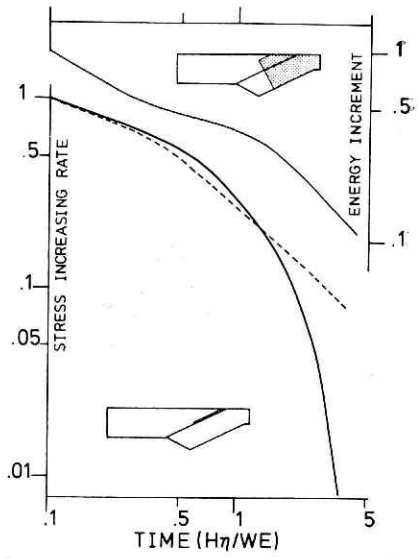

Fig. 43 Decaying curves of stress increasing rate and energy increase. The lower solid curve indicates the total stress increasing rate near the coseismic fault (dotted area). The broken curve is the modified Omori's formula fitted to the solid curve. The upper solid curve indicates time variation of the total rate of energy increase in the dotted area (upper small set).

There are a few pieces of evidence which support this suggestion. Utsu (1961) pointed out that almost all largest aftershocks occur within the first 10 days after the main shock. The largest aftershocks are not exactly regarded as random samples from such a distribution as found in the decay law of aftershock frequencies (Utsu, 1969). These suggested that the process of aftershock occurrence may undergo a change at a point about 10 days after the main shock, and that the largest and probably other larger aftershocks may be distinguished from smaller aftershocks which become more important after this time. Maki (1968, 1969) studied focal mechanisms of the 1963 Itrup (No. 1) and the 1964 Alaska (No. 2) sequences, and concluded that the shocks with a magnitude larger than about 6 have similar mechanisms to that of the main shok, but that the smaller shocks have various mechanisms. More directly, Imoto (1979) examined focal mechanisms of the July 9, 1971 sequence (No. 19)

on the basis of p wave first motion and pointed out that the shocks during **SSQA** are likely to have similar mechanisms to the main shock, and that the later shock are not necessarily the same. The result is quite interesting, and awaits more detailed research for other sequences.

6.3 Schematic view of aftershock occurrence

Up to this point, we have given an *a priori* criterion of aftershok occurrence whereby the probability density of aftershock occurrence at a certain time and position is linearly proportional to the increasing rate (counting its negative values as zero) of the shear stress at the time and position. To make a physical image of the criterion clear, the relation between stress and aftershock occurrence is shown schematically in Fig. 44.

The upper half of the figure schematically represents stress distribution relative to the fracture strength in the source region of aftershocks just after the main shock. In this exaple, the average stress drops to a far lower level than the fracture strength over almost the whole area, and yet there exists a scattering of small areas with the stress only slightly lower than the strength (Yamashita, 1974). Provisionally, we will call these small areas "*spots*". Here, we assume an uniform distribution of *spots* as functions of position and stress shortage (strength minus stress) just after the main shock, where the number of *spots* included in unit volume and unit stress shortage is a constant, ρ_0. We will explain the observed results of occurrence mentioned before by this model. If the stress recovers by $\Delta\tau(T)$ due to viscoelastic behavior of fault material during a time interval T after the coseismic slip in a unit volume while the strength does not vary, the total number of *spots* $N(T)$ where the stress exceeds the strength will be represented as follows,

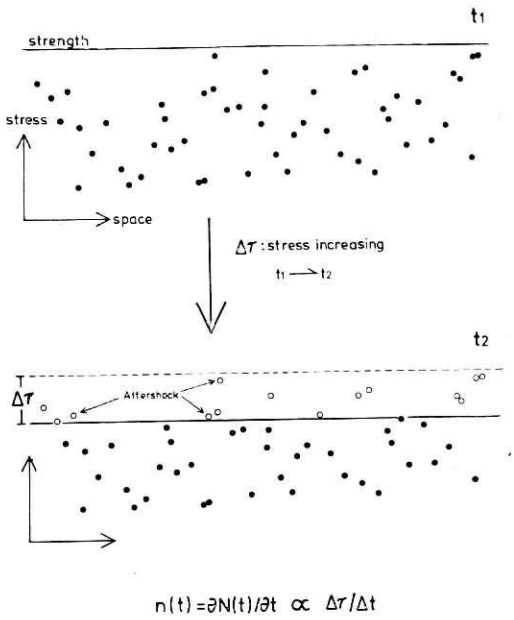

Fig. 44 Schematic view of the criterion. By coseismic slip, stress dropped to far lower than the strength (solid horizontal line) in almost all areas except for some small areas (named *spots*; closed circles in the upper diagram). Those *spots* are assumed to be uniformly distributed with respect to the variable of strength minus stress just after coseismic slip. If the stress increases by $\Delta\tau$ during the period from t_1 to t_2, the stresses at some *spots* (open circles) become larger than the strength. The frequency of aftershocks during a unit time interval, $n(t)$ is proportional to $\partial\tau/\partial t$.

$$N(T)=\rho_0\Delta\tau(T) \tag{18}$$

$$\Delta\tau(T)=\int_0^T (\partial\tau/\partial t)\,dt \tag{19}$$

T in the right-hand term of eq. (19) should be replaced by T_0, if T is longer than the transient time T_0. The above expression represents the cumulative number of aftershocks shown in Fig. 39 and 41. The frequency during a unit time interval, $n(T)$ is obtained by differenting $N(T)$ with respect to T,

$$n(T)=\partial N(T)/\partial T=\rho_0\partial\Delta\tau(T)/\partial T=\begin{cases}\rho_0\partial\tau(T)/\partial T & (\partial\tau/\partial T\geqq 0)\\ 0 & (\partial\tau/\partial T<0)\end{cases} \quad (20)$$

This representation corresponds to the frequency decay diagrams shown in Figs. 35 and 37. In our model, the shear stress $\tau(t)$ is also a function of position, and $N(T)$ and $n(T)$ vary from point to point, as have already shown. The validity of the present criterion for aftershock sequences has thus been verified, although the recovery of stress in our model is more than 10% of the stress drop on the coseismic fault, whereas the increase in static friction is estimated to be about 2-3% duriog the time from 10^5 sec to 10^6 sec (about 1 to 10 days) as seen from laboratory experiments by Dieterich (1972a, 1978).

The scheme of the present study is closely related to many theories of aftershocks which have attempted to explain the Omori's formula or its mordified form. Kusakabe (1904) attempted to interpret the Omori formula in terms of creep characteristics of rock. He derived the formula from an empirical creep function with the assumption that the aftrshock frequncy is proportional to the rate of strain recovery in rocks. Although his criterion appears similar to ours, both variation of creep characteristics and the rate of strain recovery with respect to position were not taken into consideration. Benioff (1951) proposed a mechanical model with a slider, dashpots and springs, which offers an explanation of stress recovery. However, he assumed that the source volume is common to all aftershocks and the main shock, which is not acceptable at present.

Recently, many researchers have proposed simulators to generate aftershock sequences and other seismic activity (Burridge and Knopoff, 1967 ; Otsuka, 1972). Dieterich (1972b) and Chohen (1977, 1978) simulated aftershocks on a one dimensional model with more complex parameter such as time-dependent friction. Miyatake (1977) and Mikumo and Miyatake (1978) simulated a dynamical rupture process in a quasi-three dimensional fault model. Using thess results, Miyatake (1978) and Mikumo and Miyatake (1979) successfully simulated aftershocks and earthquake sequence over a long time somewhat shorter than the recurrence time of a main shock. In their simulation of the aftershock process, many parameters such as time-dependent friction, distribution of relaxation time, strength etc. are included. Without so many parameters, our model provides a macroscopic view of aftershock process as studied by Miyatake (1978) and Mikumo and Miyatake (1979), in a similar basic line of stress concentration and stress relaxation.

The variations of frequency decay curves with distance (Figs. 18, 19 and 20) reminds us the elaborate theory by Utsu (1962), who introduced the modified Omori's formula under a certain distribution of fracture rate.

In this way, we have shown that our simple model, which is closely related to many different models, could provide successful explanations to the characteristics of aftershock occurrence.

7. Conclusions

We have investigated the spatio-temporal patterns of about thirty afterthock sequences following large thrust earthquakes in subduction zones and have found prominent migration of aftershock activity (**SSQA**) occurring for about 10 days after the main shock in many cases. In order to interpret the process of migration, the stress in the source region has been simulated by s two-dimensional finite element

model with a fault gouge which participates in viscous slip during a postseismic stage. For stress analysis, we have used an appropriate criterion in which the frequency of aftershocks is proportional to the increasing rate of the shear stress in specific time and space intervals. The main conclusions we have obtained are as follows.

(1) In general, a main shock is located on the landward side of its aftershock area. The space-time plots for the aftershock sequences show *Seaward Spreading of Quiesent Areas* in many cases. Sequences which do not show **SSQA** are located in some anomalous regions from a viewpoint of the profile of the Wadati-Benioff zone, activity of intermedite-depth earthquakes, volcanic fronts bathymetric contours and others.

(2) From the results of detailed inspections on some aftershock sequences, the following important characteristics of **SSQA** have been detected.

i) The space-time plots for a few sequences indicate that a quiescent area is more likely to start moving from a line source along the landward side of the aftershock area rather than from a point source. This evidence allows us to apply a two-dimensional approximation to model the process.

ii) Distributions of space and time intervals for an aftershock sequence show that the direction of migration is nearly normal to the trench and oriented seaward in most cases.

iii) By using a smoothing method for spatio-temporal distribution, we have found that the frequency-decaying rate of aftershocks is different from place to place and becomes slower in proportion to the distance measured seaward from the main shock.

(3) Stress histories during postseismic deformations are calculated for a number of models with different distribution of initial dislocation, boundary conditions on the bottom of the subducting plate and elastic constants in a layered or uniform structure. The histories of stress rate at several points near the fault show similar patterns for these different cases. The transient time at which the stress rate changes from an increasing to a decreasing state is proportional to the distance from a point with stress concentration just after coseismic slip. These results provide a qualitative explanation for **SSQA**.

(4) Comparisons in frequency decay curves of aftershocks at various distance points between the observed data and calculated results yield satisfactory agreements in almost all cases with **SSQA**.

(5) An analytic solution for the initial displacement with a certain functional form together with our criterion yields the freguency decay law of Omori's formula. This suggests that the gouge model proposed here may be a good approximation for producing aftershock sequences.

(6) Our results seem to be consistent with different kinds of data such as the focal mechanism of aftershocks, and origin time of the largest aftershock which is most likely to take place within 10 days after the main shock.

Acknowledgements

I wish to acknowledge the continuing guidance and encouragement of prof. Yoshimichi Kishimoto. I am very grateful to prof. Taksehi Mikumo for helpful suggestions, discussions and critical reading of the manuscript. I am indebted to Dr. Kazuo Oike for drawing my attention to this problem and for stimulating and helpful discussions. My thanks are also due to Drs. Masakazu Ohtake, Kazuo

Hamada and Hiroshi Takahashi and the staff members of our Research Division for their help and encouragement. The computations involved were made by Acos-600 at the National Research Center for Disaster Prevention.

References

1) Abe, K. (1972a) : Lithospheric nomal faulting beneath the Aleutian Trench. *Phys. Earth Planet. Interiors*, **5**, 190-198
2) Abe, K. (1972b) : Mechanisms and tectonic implications of the 1966 and 1970 Peru earthquakes. *Phys. Earth planet Interiors*, **5**, 367-379
3) Abe, K. (1973) : Tsunami and mechanism of qreat earthquakes. *Phys. Earth Planet. Inteiors*, **7**, 143-153
4) Algermissen, S. T., W.A. Rinehart, R. W. Sherburne and W. H. Dillinger, JR. (1972) : Preshocks and aftershocks. in The Great Alaska Earthquake of 1964 Seismology and Geodesy. Natonal Academy of Science, Washington, 313-364
5) Ben-Menahem, A., M. Rosenman and M. Israel (1972) : Source mechanism of the Alaska earthquake of 1964 from amplitudes of free oscilations and surface waves. *Phys. Earth planet. Interiors*, **5**, 1-29
6) Benioff, H. (1951) : Earthquake and rock creep, Part 1. Creep characterististics of rocks and the origin of aftershocks. *Bull. Seism. Soc. Amer.*, **41**, 31-62
7) Burridge, R. and L. Knopoff (1967) : Model and theoretical seismology. *Bull. Seism. Soc. Amer.*, **57**, 341-371
8) Chase, C. G. (1971) : Tectonic history of the Fiji plateau. *Geol. Soc. Amer. Bull.*, **82**, 3087-3110
9) Chung, M. Y. and H. Kanamori (1978) : Subduction Process of a fracture zone and aseismic ridges-the focal mechanism and source characteristics of the New Hebrides earthquake of 1969 January 19 and some related events. *Geophys. J. Roy. Astr. Soc.*, **54**, 221-240
10) Cohen, S. C. (1977) : Computer simulation of earthquakes. *J. Geophys. Res.*, **82**, 3781-3796
11) Cohen, S.C. (1978) : The viscoelastic stiffness model of seismicity. *J. Geophys. Res.*, **83**, 5425-5431
12) Dieterich, J. H. (1972a) : Time-dependent friction in rocks. *J. Geophys. Res.*, **77**, 3690-3697
13) Dieterich, J. H. (1972b) : Time-dependent friction as a possible mechanism for aftershocks. *J. Geophys. Soc.*, **77**. 3771-3781
14) Dieterich, J. H. (1978) : Time-dependent friction and the mechanics of stick-slip. *Pure Appl. Geophys.*, **116**, 790-806
15) Elsasser, W. M. (1969) : Convection and stress propagation in the upper mantle. in The Application of Modern Physics to the Earth and Planetary Interiors (ed. S. K. Runcorn), John Wiley, New York.
16) Fitch, T. J. (1972) : Plate convergence, transcurrent faults, and internal deformation adjacent to Southeast Asia and the Western Pacific. *J. Geophys. Res.*, **77**, 4432-4460
17) Fujii, Y. (1976) : Pre-slip as forerunner of earthquake occurrence. Proceedings of Earthquake Prediction Reseach Symposium, 127-137 (in Japanese)
18) Fujii, Y. (1978) : Phases and characteristics of seismic crustal movement with special references to Japanese earthquakes. *Bull. Geogr. Surv. Inst.*, **23**, 7-81
19) Fujii, Y. (1979) : Abstracts, annual meeting, Seismological Society of Japan (in Japanese)
20) Fukao, Y. (1977) : Abstracts, annual meeting, Seismological Society of Japan (in Japanese)
21) Fukao, Y. (1979) : Tsunami earthquakes and subduction processes near deep-sea trenches. *J. Geophy. Res.*, **84**, 2303-2314
22) Grow, J. A. (1973) : Crustal and upper mantle structure of the central Aleutian arc. *Geol. Soc. Amer. Bull.*, **84**, 2169-2192

23) Harding, S. T. and S. T. Algermissen (1969) : Focal mechanism of the Prince Willam Sound, Alaska earthquake of March 28, 1964. *Bull. Seism. Soc. Amer.*, **59**, 799-811
24) Hatori, T. (1970) : An investigation of the tsunami qenerated by the East Hokkaido earthquake of August, 1969. *Bull. Earthquake. Res. Inst.*, **48**, 399-412
25) Ichikawa, M. (1973) : Abstracts, annual meeting, Seismological Society of Japan (in Japanese)
26) Ida, Y. (1974) : Slow-moving deformation pulses along tectonic faults. *Phys. Earth Planet. Interiors*, **9**, 328-337
27) Iida, K. (1956) : Earthquakes accompanied by tsunamis occuring under the sea off the island of Japan. *J. Earth Science Nagoya Univ.*, **4**, 1-43
28) Imoto, M. (1976) : On a staring point of the large fracture of August 11, 1969. Hokkaido Toho-oki earthquake. *Zisin, Ser.* II, **29**, 1-13 (in Japanese)
29) Imoto, M. and Y. Kishimoto (1977a) : On a bias of aftershock epicenters at trenches of the Pacific Ocean. *Disas. Prev. Res. Inst. Kyoto. Univ. Annals*, **20 B-1**, 59-67 (in Japanese)
30) Imoto, M. and Y. Kishimoto (1977b) : Statistical search for migrations of aftershock sequences. *Bull. Disas. Prev. Res. Inst. Kyoto Univ.*, **27**, 93-111
31) Imoto, M. (1979) : Abstracts, annual meeting, Seismlogical Society of Japan (in Japanese)
32) Isacks, B. L., L. R. Sykes and J. Oliver (1967) : Spatial and temporal clustering of deep and shallow earthquakes in the Fiji-Tonga-Kermadec region. *Bull. Seism. Soc. Amer.*, **57**, 935-958
33) Isacks, B. L., L. R. Sykes and J. Oliver (1969) : Focal mechanisms of deep and shallow earthquakes in the Tonga-Kermadec region and the tectonics of islands arcs. *Geol. Soc. Amer. Bull.*, **80**, 1443-1470
34) Isacks, B. L. and M. Barazangi (1977) : Geometry of Benioff zones : Lateral segmentation and downwards bending of the subducted lithosphere. in Island Arcs, Deep Sea Trenches, and Back-Arc Basins, Maurice Ewing Ser. 1, (ed. M.Talwani and W. C. Pitman III), 99-114
35) Isacks, B. L. and P. Molnar (1971) : Distribution of stresses in the descending lithosphere from a global survey of focal-mechanism solution of mantle earthquakes. *Rev. Geophys. Space Phys.*, **9**, 103-174
36) Ishimoto, M. (1937) : On the occurrence of aftershocks and crustal deformation. *J. Seism. Soc. Japan(Zisin)*, **9**, 108-117 (in Japanese)
37) Johnson, T. and P. Molnar (1972) : Focal mechanisms and plate tectonics of the Southwest Pacific. *J. Geophys. Res.*, **77**, 5000-5031
38) Jungels, P. H. and G. A. Frazier (1973) : Finite element analysis of the residual displacements for an earthquake rupture : Source parameters for the San Fernando earthquake. *J. Geophys. Res.*, **78**, 5062-5083
39) Kanamori, H. (1970a) : Synthesis of long-period surface waves and its application to earthquake source studies-Kurile Islands earthquake of October 13, 1963. *J. Geophys. Res.*, **75**, 5011-5027
40) Kanamori, H. (1970b) : The Alaska earthquake of 1964 : Radiation of long surface waves and source mechanism. *J. Geophys. Res.*, **75**, 5029-5040
41) Kanamori, H. (1970c) : Velocity and Q of mantle waves. *Phys. Earth Planet. Interiors*, **2**, 259-275
42) Kanamari, H. (1971a) : Focal mechanism of the Tokachi-Oki earthquake of May 16, 1968 : Contortion of the lithosphere at a junction of two trenches. *Tectonophysis*, **12**, 1-13
43) Kanamori, H. (1971b) : Great earthquakes at islands arcs the lithosphere. *Tectnophysics*, **12**, 187-198
44) Kanamri, H. (1972) : Tectonic implications of the 1944 Tonankai and 1946 Nankaido earthquakes. *Phys. Earth Planet. Interiors*, **5**, 129-139
45) Kanamori, H. (1973) : Mode of strain release associated with major earthquakes in Japan. in Annual Riview of Earth Planetary Science, **1**, (ed. F. A. Donath), 213-239

46) Kanamori, H. and J. J. Cipar (1974) : Focal process of the great Chilean earthquake May 22, 1960. *Phys. Earth Planet. Interiors*, **9**, 128-136

47) Kanamori, H. (1977) : Seismic and aseismic slip along subduction zones and their tectonic implications. in Island Arcs, Deep Sea Trenches, and Back-Arc Basins, Maurice Ewing Ser. 1 (ed. M. Talwani and W. C. Pitman III), 163-174, AGU, Washington

48) Kasahara, K. (1975) : Aseismic faulting follwing the 1973 Nemoro-Oki earthquake, Hokkiado, Japan (a possibility) in Earthquake Prediction and Rock Mechanics, Contribution to Current Research in Geophysics (CCRG)1(ed. M. Wyss), 127-139, Birhauser

49) Kato, T. and K. Tsumura (1979) : Vertical inland movement in Japan as deduced from tidal record. *Bull. Earthq. Res. Inst.*, 54, 559-628

50) Kelleher, J., L. R. Sykes and J. Oliver (1973) : Possible criteria for predicting earthquake locations and their application to major plate boundries of the Pacific and Caribbean. *J. Geophys.*, **78**, 2547-2585

51) Kelleher, J. and W. McCann (1976) : Buoyant zones, great earthquakes, and unstable boundaries of subduction. *J. Geophys. Res.*, **81**, 4885-4896

52) Kelleher, J. and W. McCann(1977) : Bathymetric highs and the development of convergent plate boundaries. in Island Arcs, Deep Sea Trenches and Basins, Maurice Ewing Ser. 1 (ed. M. Talwani and W. C. Pitman III), 115-122, AGU, Washington

53) Kishinouye, F. (1936) : Distribution of earthquakes before and after the Izu earthquake of 1930. *J. Seism. Soc. Japan (Zisin)*, 7, 585-591

54) Kusakabe, S. (1904) : Modulus of elasticity of rocks and velocity of seisomic waves with a hint to the frequency of aftershocks. *Pub. Earthq. Inv. Comm.*, **17**, 1-48

55) Maki, T. (1968) : Focal mechanisms of the 1963 Itrup earthquake sequene. *Geophys. Bull. Hokkaido Univ.*, **19** 21-55

56) Maki, T. (1969) : Focal mechanism of the 1964 Alaska earthquake sequence. *Geophys. Bull. Hokkaido Univ.*, **21**, 63-105

57) Malfait, B. T. and M. G. Dinkelman (1972) : Circum-Caribbean tectonic and igneous activity and the evolution of the Caribbean plate. *Geol. Soc. Amer. Bull.*, **83**, 251-272

58) Melosh, H. J. (1976) : Nonlinear stress propagation in the earth' s upper mantle. *J. Geophys. Res.*, **81**, 5621-5632

59) Melosh, H. J. (1978) : Reply. *J. Geophys. Res.*, **83**, 5009-5010

60) Mikumo, T.(1968) : Atmospheric pressure waves and tectonic deformation associated with the Alaskan earthquake of March 28, 1964. *J. Geophys. Res.*,**73**, 2009-2025

61) Mikumo, T. (1973) : Faulting process of the San Fernando earthquake of February 9, 1971, inferred from static and dynamic near-field displacements. *Bull. Seism. Soc. Amer.* **63**, 249-269

62) Mikumo, T. and T. Miyatake (1978) : Dynamical rupture process on a three-dimensional fault with non-uniform frictions and near-field seismic waves. *Geophys. J. Roy. Astro. Soc.*, **54**, 417-438

63) Mikumo, T. and T. Miyatake (1979) : Earthquake sequences on a frictional fault model with non-uniform strengths and relaxation times. *Geophys. J. Roy. Astro. Soc.*, **59**, 497-522

64) Mitronovas, W., B. L. Isacks and L. Seeber (1969) : Earthquake locations and seismic wave propagation in the upper 250 km of the Tonga Island arc. *Bull. Seism. Soc. Amer.*, **59**, 1115-1135

65) Miyashita, K. and M. Matsu'ura (1978) : Inversion analysis of static displacement data associated with the Alaska earthquake of 1964. *J. Phys. Earth*, **26**, 333-349

66) Miyatake, T. (1977) : Numerical simulation of dynamic rupture process. *Zisin, Ser.* II, **30**, 449-461 (in Japanese)

67) Miyatake, T. (1978) : Numerical simulation aftershock procss. *Zisin, Ser.* II, **31**, 161-177 (in Japanese)

68) Mogi, K. (1962a) : On the time distribution of aftershocks accompanying the recent major earthquakes in and near Japan. *Bull. Earthq. Ses. Inst.*, **40**, 107-124

69) Mogi, K. (1962b) : Study of elastic shocks caused by the fracture of heterogeneous materials and its relation to earthquake phenomena. *Bull. Earthq. Res. Inst.*, **40**, 125-173

70) Mogi, K. (1962c) : The fracture of fracture of a semi-infinite body caused by an inner stress origin and its relation to the earthquake phenomena (First paper). *Bull. Earthq. Res. Inst.*, **40**, 815-829

71) Mogi, K. (1963a) : The fracture of a semi-infinite body caused by an inner stress origin and its relation to the earthquake phenomena (Second paper) - The case of the materials having some heterogeneous structures-. *Bull. Earthq. Res. Inst.*, **41**, 595-614

72) Mogi, K. (1963b) : Some discussions on aftershocks, foreshocks and earthquake swarms - The fracture of a semi-infinite body caused by an inner stress origin and its relation to the earthquake phenomena (Third paper). *Bull. Earthq. Res. Inst.* **41**, 615-658

73) Mogi, K. (1968) : Development of aftershock area of great earthquakes. *Bull. Earthq. Res. Inst.*, **46**, 175-203

74) Molnar, P. and L. R. Sykes (1969) : Tectonics of the Caribbean and Middle America regions from focal mechanisms and seismicity. *Geol. Soc. Amer. Bull.*, **80**, 1639-1684

75) Oike, K. (1971) : On the nature of the occurrence of intermediate and deep earthquakes, 2 Spatial and temporal clustering. *Bull. Disas. Prev. Res. Inst., Kyoto Univ.*, **21**, 43-73

76) Okada, Y. (1980) : Theoretical strain seismogram and its applications. *Bull. Earthq. Res. Inst.*, **55**, 101-168 (in Japanese)

77) Otsuka, M. (1972) : A simulation of earthquake occurrence. *Phys. Earth Planet. Interiors*, **6**, 311-315

78) Pascal, G., B. L. Isacks, M. Barazangi and J. Dubois (1978) : Precise relocations of earthquake and seismotectonics of the New Hebrides island arc. *J. Geophys. Res.*, **83**, 4957-4973

79) Pascal, G. (1979) : Seismotectonics of the papua New Guinea -Solomon Island region. *Tectonophysics*, **57**, 7-34

80) Plafker, G. (1969) : Tectonics of the March 27, 1964, Alaska Earthquake. *U. S. Geol. Surv. Prof. Pap.*, **534-I**

81) Press, F. (1965) : Displacements, strains, and tilts at teleseismic distances. *J. Geophys. Res.*, **70**, 2395-2412

82) Research Group of Explosion seismology (1977) : Regionality of the upper mantle around northeastern Japan as derived from explosion seismic observations and its seismological implications. *Tectonophysics*, **37**, 117-130

83) Ripper, I. D. (1975) : Some earthquake focal mechanisms in the New Guinea Solomon Islands region 1969-1971. *Bur. Miner. Resour. Aust. Bulletin*

84) Santo, T. (1964) : Shock sequence of the southern Kurile Islands from October 09 to December 31, 1963. *Bull. Internat. Inst. Seism. Earthq. Eng.*, **1**, 33-54

85) Santo, T. (1970a) : Regional study on the characteristic seismicity of the world : Part III -New Hebrides Islands regions. *Bull. Earthq. Res. Inst.*, **48**, 1-18

86) Santo, T. (1970b) : Regional study on the characteristic seismicity of the world. Part VII Activity of aftershocks in Kurile Islands region. *Bull. Internat. Inst. Seism. Earthq.*, Eng. **7**, 119-131

87) Savage, J. C. and L. M. Hastie (1966) : Surface deformation associated with dip-slip faulting. *J. Geophys. Res.*, **71**, 4897-4904

88) Savage, J. C. and W. H. Prescott (1978) : Comment on "Non-linear stress propagation in the earth's upper mantle" by H. J. Melosh. *J. Geophys. Res.*, **83**, 5005-5007

89) Scholz, C. H. (1968) : Microfracture, aftershocks, and seismicity. *Bull. Seism. Soc. Amer.*, **58**, 1117-1130

90) Sclater, J. G., D. Karig, L. A. Lawver and K. Louden (1976) : Heat flow, depth, and crustal thickness of the marginal basins of the south Philippine sea. *J. Geophys. Res.*, **81**, 309-318

91) Seno, T. and K. Kurita (1978) : Focal mechanisms and tectonics in the Taiwan-Philippine region. *J. Phys. Earth*, **26**, Suppl., 249-263

92) Shimazaki, K. (1974a) : Pre-seismic crustal deformation caused by an underthrusting oceanic plate, in eastern Hokkaido Japan. *Phys. Earth planet. Interiors*, **8**, 148-157

93) Shimazaki, K. (1974b) : Nemuro-Oki earthquake of June 17, 1973 : A lithospheric rebound at the upper half of the interface. *Phys. Earth Planet. Interiors*, **9**, 314-327

94) Stauder, W. and G. A. Bollinger (1966) : The focal mechanism of the the Alaska earthquake of March 28, 1964 and of its aftershock sequence. *J. Geophys. Res.*, **71**, 5283-5296

95) Stauder, W. (1968) : Mechanism of the Rat Island earthquake sequence of February 4, 1965, with relation to island arcs and sea-floor spreading. *J. Geophys. Res.*, **73**, 3847-3858

96) Stauder, w. (1973) : Mechanism and spatial distribution of Chilean earthquakes with relation to subduction of the oceanic plate. *J. Geophys. Res.*, **78**, 5033-5061

97) Stauder, w. (1975) : Subduction of the Nazca Plate under Peru as evidenced by focal mechanisms and by seismicity. *J. Geophys. Res.*, **80**, 1053-1064

98) Stauder, W. and L. Maulchin (1976) : Fault motion in the larger earthquakes of the Kurile-Kamchatcka arc and the Kurile-Hokkaido corner. *J. Geophys. Res.*, **81**, 297-308

99) Sykes, L. R. (1966) : The seismicity and deep structure of islands arcs. *J. Geophys. Res.*, **71**, 2981-3006

100) Tada, T. (1974a) : Fault model and crustal movement of the 1973 Nemuro-Oki earthquake. *Zisin, Ser.*II, **27**, 120-128 (in Japanese)

101) Tada, T. (1974b) : Crustal movement and fault motion associated with the 1973 Nemuro-Oki earthquake. *Bull. Geogr. Surv. Inst.*, **20**, 175-186

102) Thatcher, W. (1975) : Strain accumulation and release mechanism of the 1906 San Francisco earthquake. *J. Geophys. Res.*, **80**, 4862-4872

103) Thatcher, W. and J. B. Rundle (1979) : A model for the earthquake cycle in underthrust zones. *J. Geophys. Res.*, **84**, 5540-5556

104) Utsu, T. and A. Seki (1955) : Relation between the area of aftershock region and the energy of main shock. *Zisin, Ser.*II, 7, 233-240 (in Japanese)

105) Utsu, T. (1961) : A statistical study an the Occurrence of aftershocks. *Geophys. Mag.*, **30**, 521-605

106) Utsu, T. (1962) : On the nature of Alaskan aftershock sequences of 1957 and 1958. *Bull. Seism. Soc. Amer.*, **52**, 279-297

107) Utsu, T. (1967) : Anomalies in seismic wave velocity attenuation associated with a deep earthquake zone (I). *J. Fac. Sci. Hokkaido Univ., Ser.*VII, **3**, 1-25

108) Utsu, T. (1969) : Aftershocks and earthquake statistics (I). *J. Fac. Sci. Hokkaido Univ., Ser.* VII ,**3**, 129-195

109) Utsu, T. (1970) : Aftershocks and earthquake statistics (II). *J. Fac. Sci. Hokkaido Univ., Ser.* VII, **3**, 197-266

110) Ustu, T. (1971a) : Seismological evidence for anomalous structure of island arcs with special reference to the Japanese region. *Rev. Geophys. Space Phys.*, **9**, 839-890

111) Utsu, T. (1971b) : Aftershocks and earthquake statistics (III). *J. Fac. Sci. Hokkaido Univ., Ser.* VII, **3**, 379-441

112) Utsu, T. (1972) : Aftershocks and earthquake statistics (IV). *J. Fac. Sci. Hokkaido Univ., Ser.* VII, **4**, 1-42

113) Uyeda, S. and K. Horai (1964) : Terrestrial heat flow in Japan, *J. Geophys. Res.*, **69**, 2121-2141

114) Whitcomb, J. H., C. R. Allen, J. D. Garmany and J. A. Hileman (1973) : San Fernando earthquake series, 1971 : Focal mechanisms and tectonics. *Rev. Geophys. Space Phys.*, **11**, 693-730

115) Wilson, E. L. and R. W. Clough (1962) : Dynamic response by a step by step analysis. Proc. SymPosium on the use of computers in civil engineering, Lisbon

116) Wu, F. T. and H. Kanamori (1973) : Source mechanism of February 4, 1965, Rat Island earthquake. *J. Geophys. Res.*, **78**, 6082-6092

117) Wyss, M. and J. N. Brune (1967) : The Alaska earthquake of 28 March 1964, A complex multiple rupture. *Bull. Seism. Soc. Amer.*, **57**, 1017-1023

118) Yamada, J. and K. Kasahara (1975) : Continuous observation of crustal movement at Matsuyama, Shikoku, Japan. *J. Geod. Soc. Japan*, **21**, 91-97 (in Japanese)

119) Yamakawa, N. (1965) : Some investigations of aftershocks (I), Local concentration of aftershock energy and crustal deformation accompanying the main shock. Zisin, Ser, II, **18**, 25-40 (in Japanese)

120) Yamakawa, N. (1966) : Foreshocks, aftershocks and earthquake swarms (I). *Met. Geophys.*, **17**, 157-189

121) Yamakawa, N. (1967a) : Foreshocks, aftershocks and earthquake swarms (II). *Met. Geophys.*, **18**, 15-26

122) Yamakawa, N. (1967b) : Foreshocks, aftershocks and earthquake swarms (III). *Met. Geophys.*, **18**, 77-88

123) Yamakawa, N. (1968a) : Foreshocks, aftershocks and earthquake swarms (IV). *Met. Geophys.*, **19**, 109-119

124) Yamakawa, N. (1968b) : Foreshocks, aftershocks and earthquake swarms (V). *Met. Geophys.*, **19**, 437-445

125) Yamakawa, N., M. Kishio and K. Abe (1969) : Spatial and time distributions of foreshocks and aftershocks of the earthquake near the southern Kurile on 13 October 1963. *Geophys. Mag.*, **34**, 277-306

126) Yamakawa, N. (1971) : Aftershocks and focal mechanism of main shocks. *Geophys. Mag.*, **36**, 15-30

127) Yamakawa, N. and M. Kishio (1972) : Aftershocks of the Tokachi-Oki earthquake 1968 (I) -relation between the aftershock activity and the focal mechanisms of the main shock-. *Geophys. Mag.*, **36**, 1-13

128) Yamakawa, N., M. Kishio and I. Maeda (1972) : Aftershocks of the Tokachi-Oki earthquake of 1968 (II) - Spatial and temporal distributions of the aftershocks and the focal mechanisms of the main shock and major aftershocks-. *Geophys. Mag.*, **36**, 53-73

129) Yamashita, T. (1979) : Aftershock occurrence due to viscoelastic stress recovery and an estimate of the tectonic stress field near the San Andreas fault system. *Bull. Seism. Soc. Amer.*, **69**, 661-687

(Manuscript received November 26, 1980)

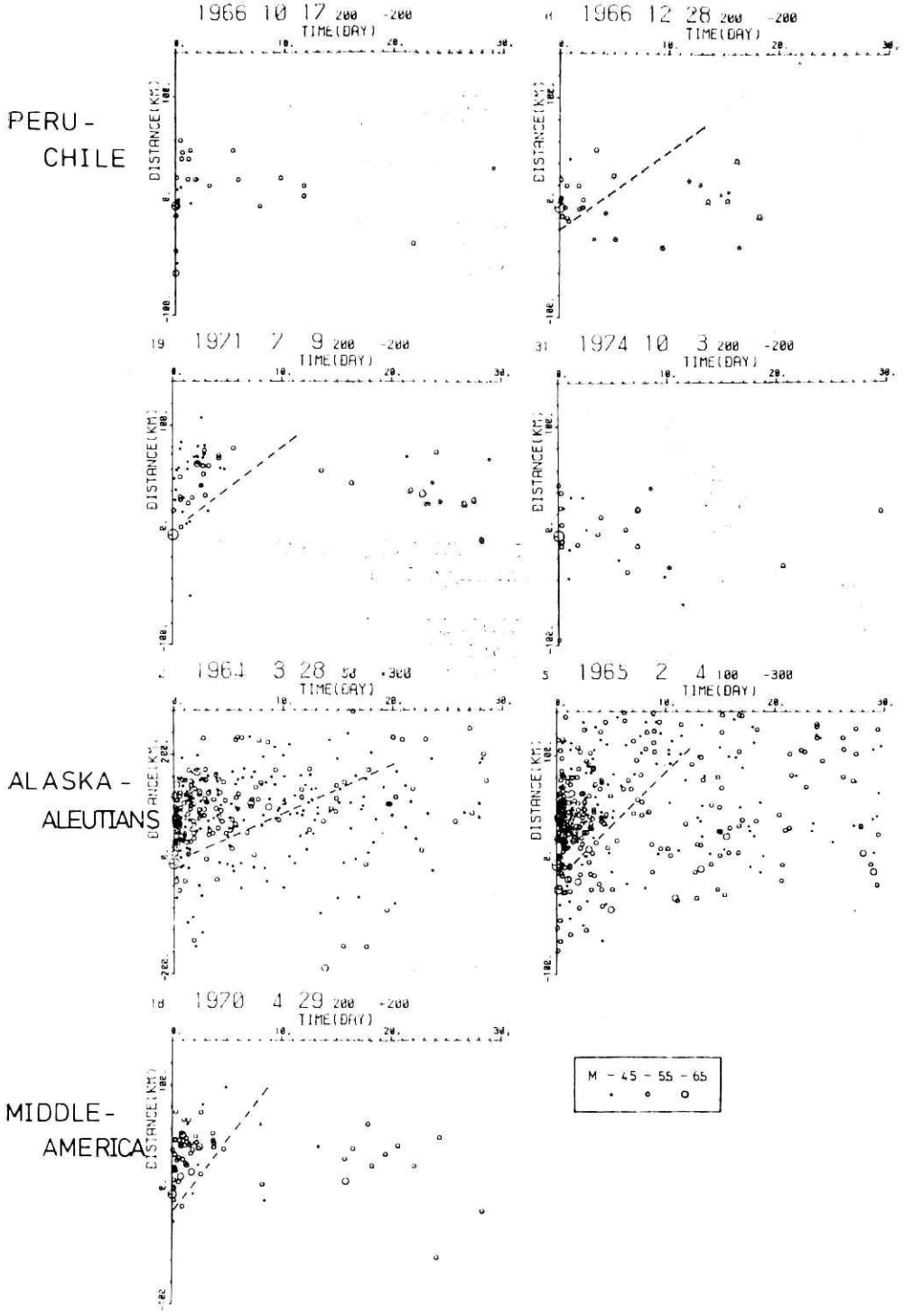

Appendix 1 Space-time plots, *in kilometers and days.* For the sequences showing **SSQA**, dashed lines indicate linear approximations for the fronts of **SSQA**, which are derived from theoretical frequency-time curves.

KURILES

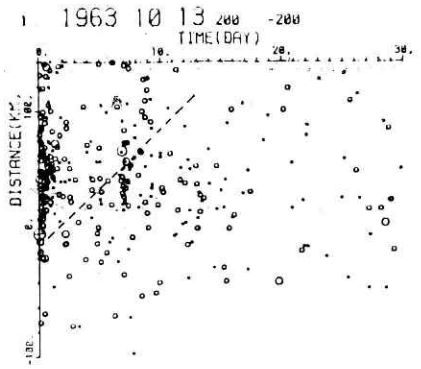

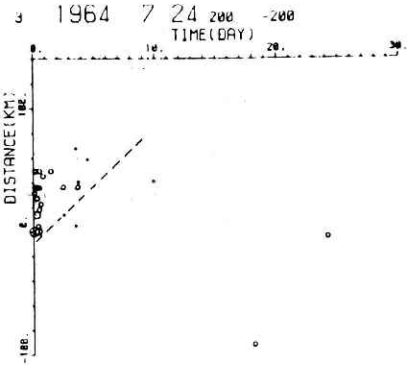

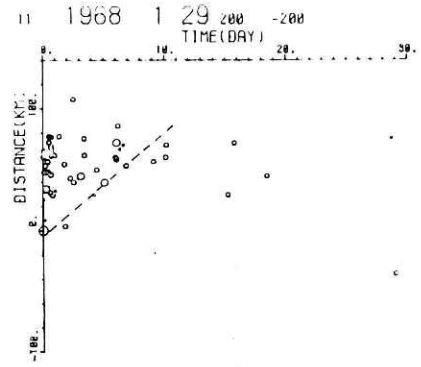

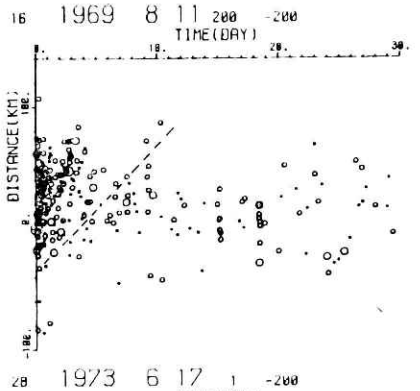

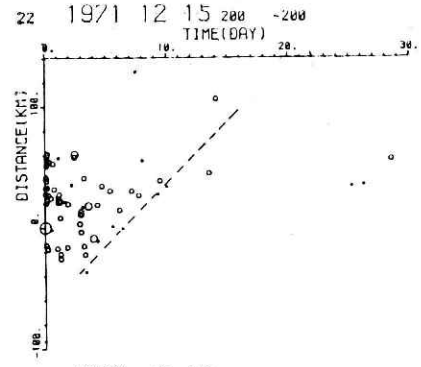

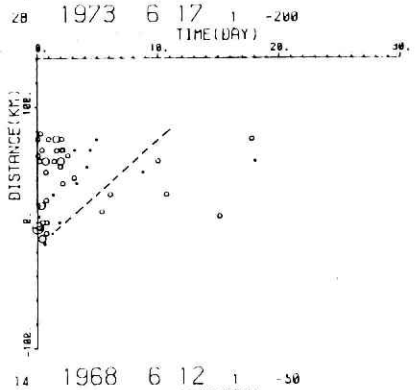

JAPAN

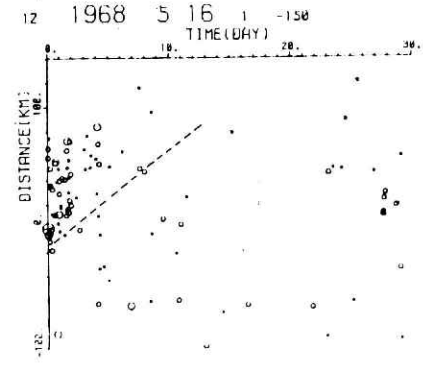

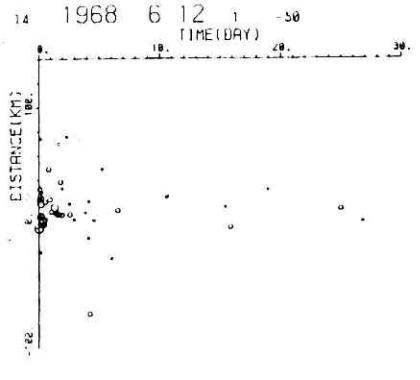

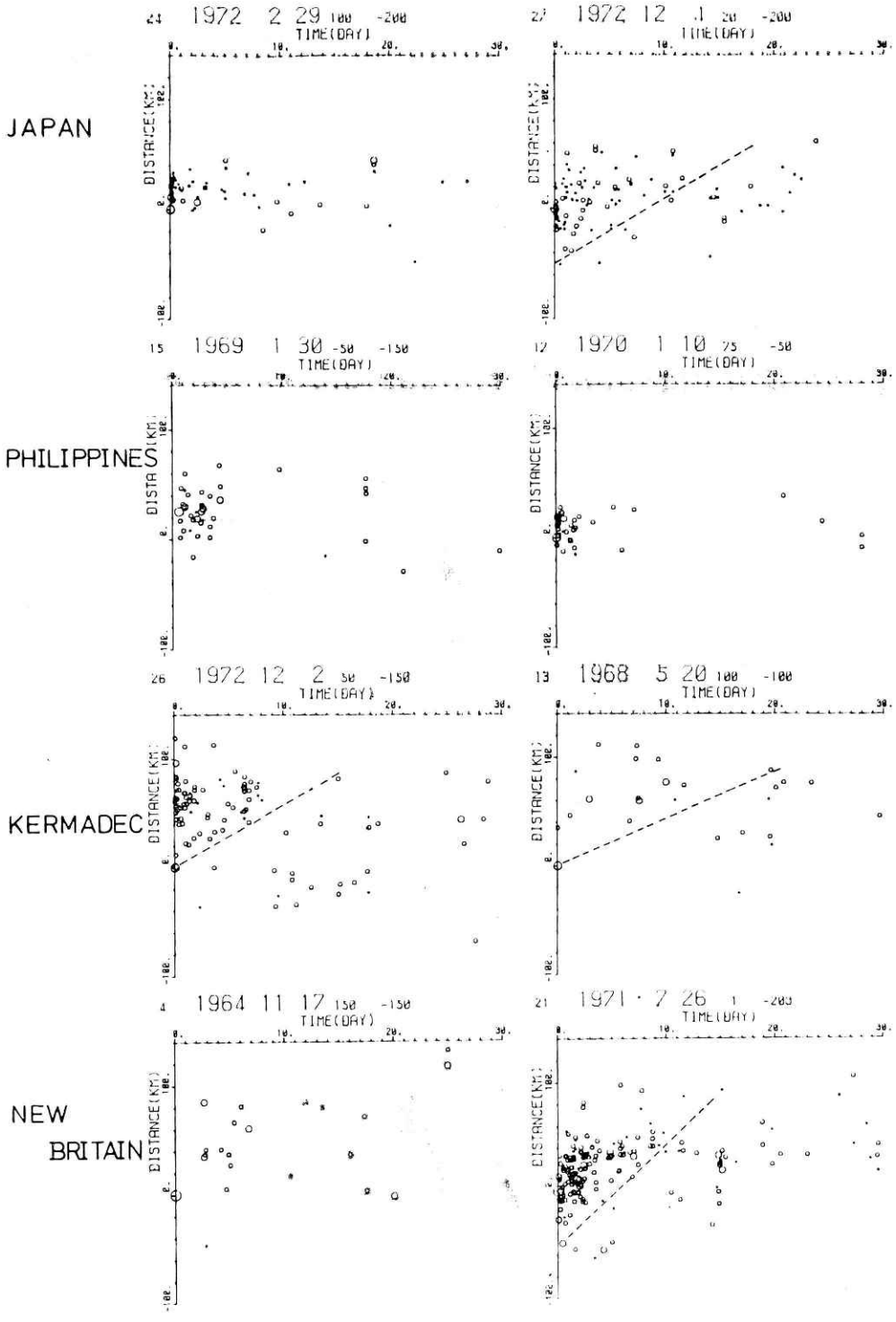
JAPAN
PHILIPPINES
KERMADEC
NEW BRITAIN
TIME(DAY)
DISTANCE(KM)

SOLOMONS

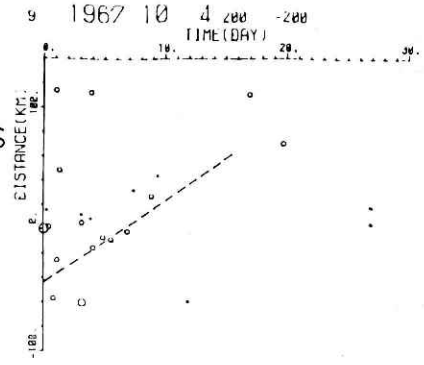

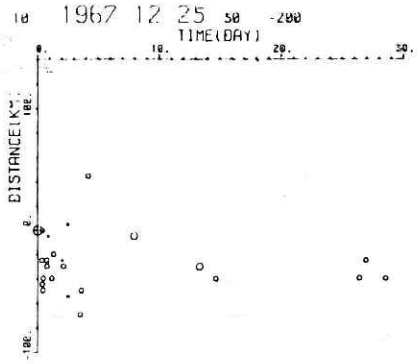

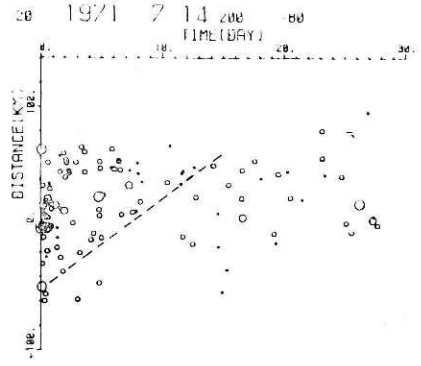

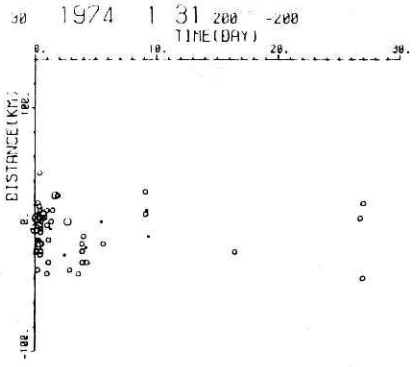

NEW HEBRIDES

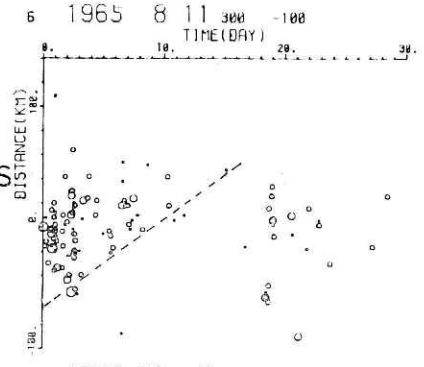

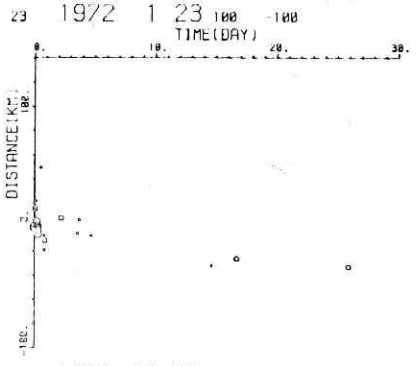

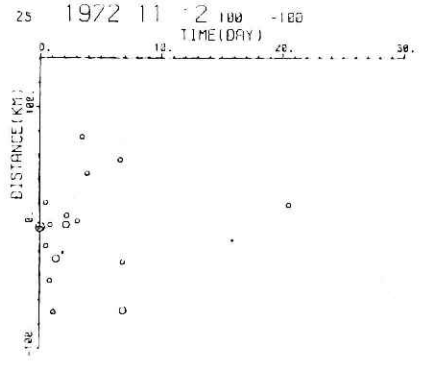

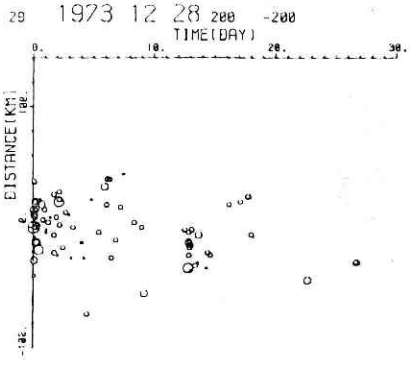

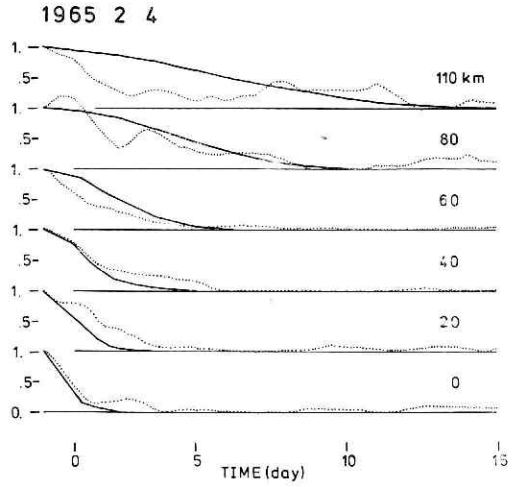

Appendix 2 Theoretical and observed frequency-time curves at several distance ranges.

For the sequences showing **SSQA** except for those displayed in section 5.5, theoretical frequency decaying curves (for No. 5) and cumulative frequency curves, indicated by solid lines, are compared with observed data.

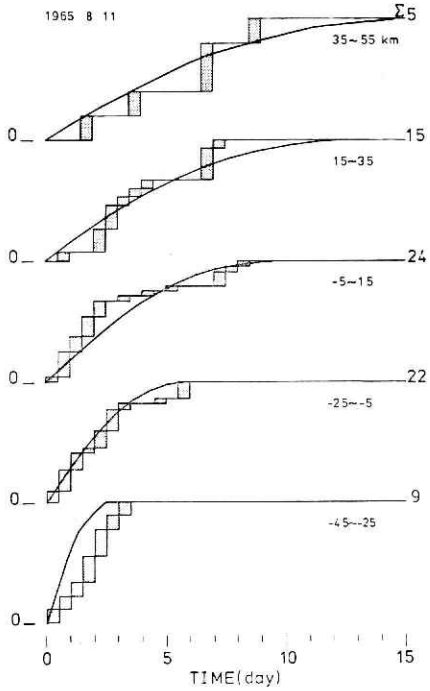

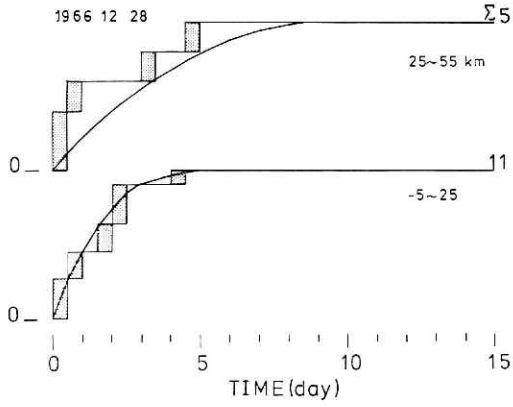

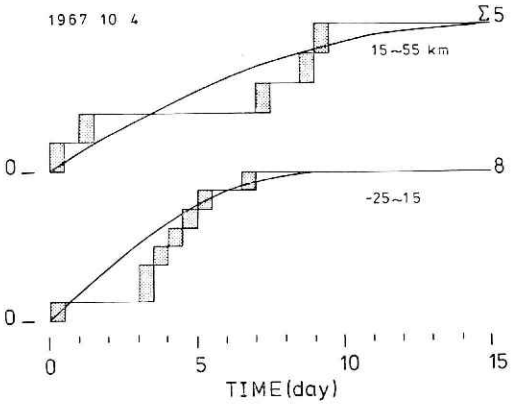
1967 10 4
Σ5
15~55 km
0
8
-25~15
0
0
5
10
15
TIME(day)

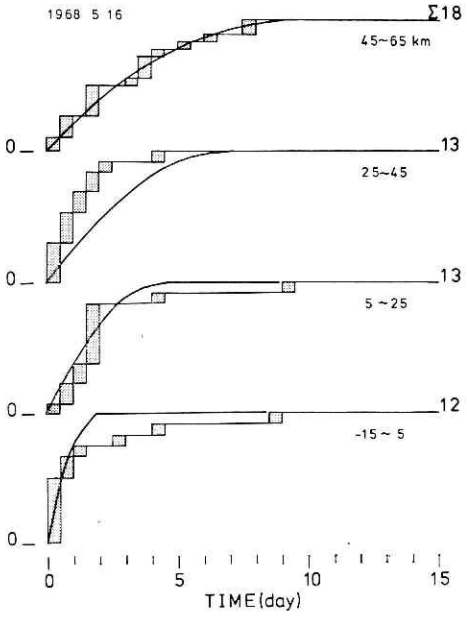
1968 5 16
Σ18
45~65 km
0
13
25~45
0
13
5 ~25
0
12
-15 ~ 5
0
0
5
10
15
TIME(day)

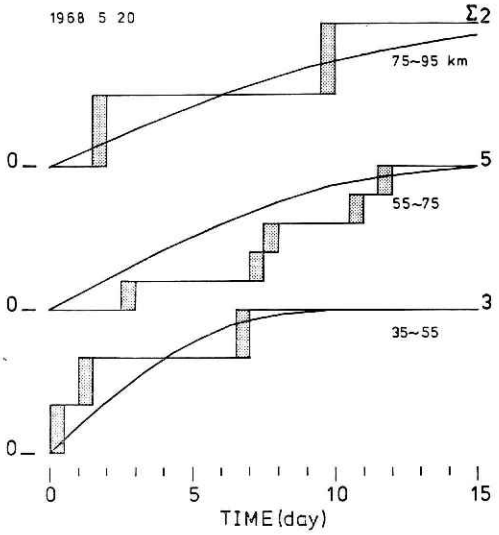
1968 5 20
Σ2
75~95 km
0
5
55~75
0
3
35~55
0
0
5
10
15
TIME(day)

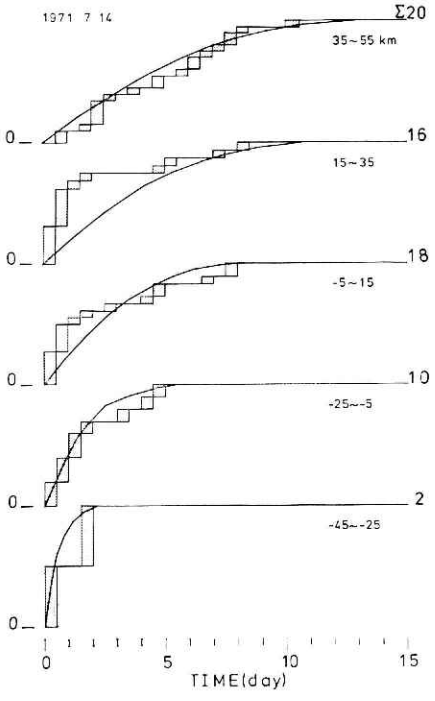
1971 7 14
Σ20
35~55 km
0
16
15~35
0
18
-5~15
0
10
-25~-5
0
2
-45~-25
0
0
5
10
15
TIME(day)

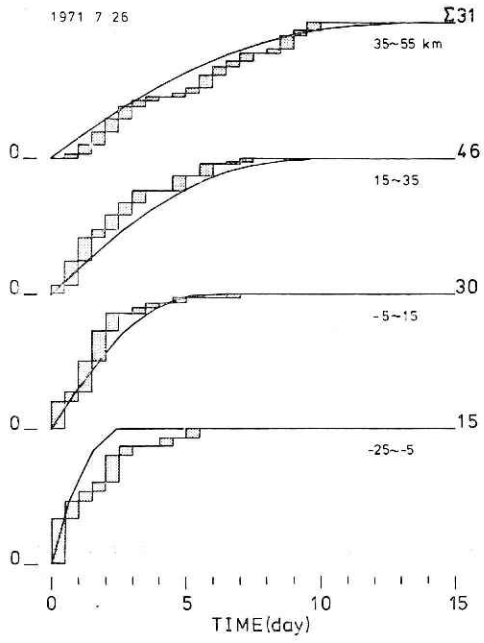
1971 7 26
Σ31
35~55 km
46
15~35
30
-5~15
15
-25~-5
0
5
10
15
TIME(day)

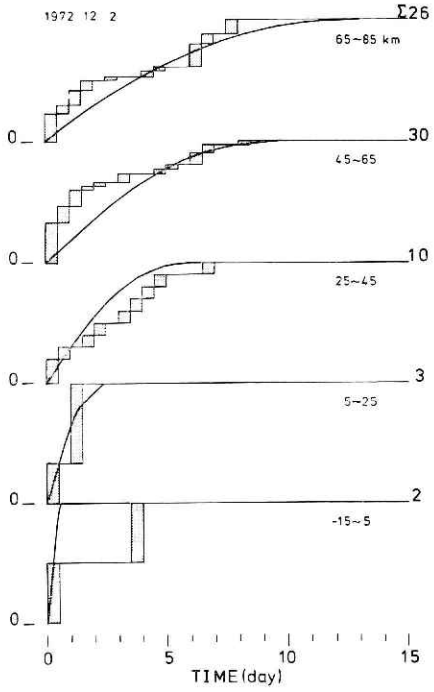
1972 12 2
Σ26
65~85 km
30
45~65
10
25~45
3
5~25
2
-15~5
0
5
10
15
TIME(day)

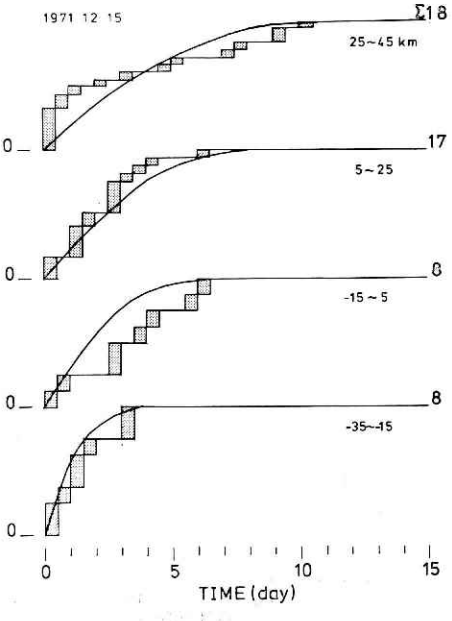
1971 12 15
Σ18
25~45 km
17
5~25
8
-15~5
8
-35~-15
0
5
10
15
TIME(day)

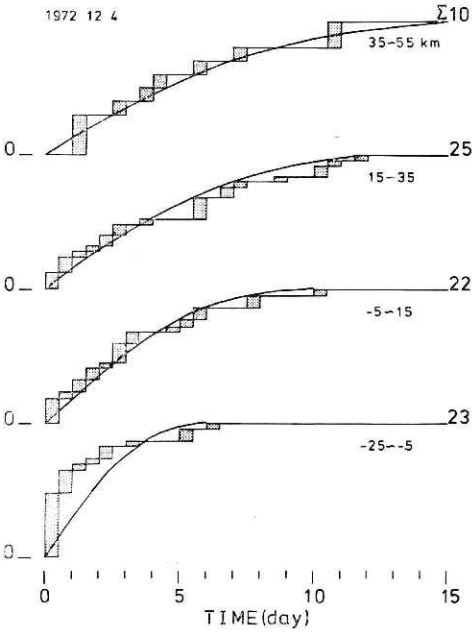
1972 12 4
Σ10
35~55 km
25
15~35
22
-5~15
23
-25~-5
0
5
10
15
TIME(day)

プレートの沈み込み帯における逆断層型大地震に伴う余震活動の移動現象について

井元政二郎*

国立防災科学技術センター

環太平洋の海溝沿いに発生する逆断層型大地震（$M \geqq 7.0$）に伴う余震活動31例について時空分布を調査した．本震後約30日間の活動を調査対象とした．31例中19例に共通して，余震活動の移動現象が見出された．この現象の特徴は，余震活動の不活発な地域が余震域の陸側端に発生し，漸次海溝に向って拡大（速度6—13km/day）して，およそ10日間で余震域全体を覆うこと（SSQA）である．SSQA の性質を調べた結果は次の様である．

(1) 深発地震面の形状，稍深発地震の活動状態，火山列あるいは海底地形に関して，島弧海溝系としては異常な場所では，SSQAは出現しにくいものと思われる．

(2) 海溝沿いに長く伸びた余震域をもつ活動を，海溝に直交する面で分割し，それぞれに対して時空分布図を作ると，類似したSSQA が認められる．このことから，SSQA は海溝に沿う方向には関係せず，二次元問題として取扱い得ることがわかる．

(3) 余震相互の時間間隔空間距離の分布を調べることにより，活動の移動方向を客観的に判断できる．余震数の比較的多い活動に対して調査した結果，移動の方向は海溝に直交し海に向う方向が最も卓越している．

(4) 時空分布をやや平滑化する処理を行なって，余震発生数減衰の海溝からの距離による違いを調べた．その結果，陸に近い地域では減衰が急で，海溝に近づくにつれて緩やかになることがわかった．

沈み込み帯におけるプレート境界面（断層）は粘性物質とし，両側のプレートは完全弾性体とした，海溝に直交する二次元粘弾性体モデルについて，震源域における応力分布を二次元有限要素法により求め，応力と余震発生の関係を調べた．本震断層面深部延長（プレート境界面の一部）における前駆的なすべりと本震時のすべりにより，本震断層面深部端付近に応力集中が発生する．この応力集中の解放が断層面における粘性的なすべりにより行なわれるとする．この本震後の変動に伴う応力の履歴を，初期条件，境界条件，弾性定数の分布を考慮し，いくつかの例について計算した．単位時間の余震発生数は応力再分配過程での応力増加率に比例すると仮定し，次の結果を得た．

(5) 断層近傍の点における応力増加量の時間変化は，条件の差異にもかかわらずほぼ同様

* 第2研究部地震活動研究室

の履歴を示す．応力増加の状態から減少の状態に移る時刻（これ以後余震は発生しなくなると考えられる）は，応力集中点から離れるに従って遅れる．

(6) 海溝までの距離の異なるいくつかの地点における余震発生数の減衰曲線について，観測値と計算による期待値を比較した結果，満足すべき一致が見られた．

さらに次の様な考察を行なった．

(7) 二次元半無限弾性体に挟まれた粘性的断層面上に，デルタ関数型くい違い変位が初期条件として存在する場合の応力場を解析的に求めた．得られた応力場に対して，先に仮定した余震発生と応力場の関係を用いると，余震発生数に関する大森公式が導かれた．

(8) 本研究の結果は，余震のメカニズムや最大余震の発生時刻（本震後10日以内になることが多い）の研究結果と調和的である．